Peridotite Melting at 1 GPa: Reversal Experiments on Partial Melt Compositions Produced by Peridotite–Basalt Sandwich Experiments

Article *in* Journal of Petrology · December 2001

DOI: 10.1093/petrology/42.12.2363

1 author:

Trevor J. Falloon
University of Tasmania
94 PUBLICATIONS **6,144** CITATIONS

SEE PROFILE

JOURNAL OF PETROLOGY | VOLUME 42 | NUMBER 12 | PAGES 2363–2390 | 2001

Peridotite Melting at 1 GPa: Reversal Experiments on Partial Melt Compositions Produced by Peridotite–Basalt Sandwich Experiments

TREVOR J. FALLOON[1]*, LEONID V. DANYUSHEVSKY[1] AND DAVID H. GREEN[2]

[1]SCHOOL OF EARTH SCIENCES, UNIVERSITY OF TASMANIA, GPO BOX 252-79, HOBART, TAS. 7001, AUSTRALIA

[2]RESEARCH SCHOOL OF EARTH SCIENCES, AUSTRALIAN NATIONAL UNIVERSITY, CANBERRA, A.C.T. 0200, AUSTRALIA

RECEIVED JANUARY 31, 2000; REVISED TYPESCRIPT ACCEPTED JUNE 25, 2001

One of the goals of igneous petrology is to use the subtle and more obvious differences in the geochemistry of primitive basalts to place constraints on mantle composition, melting conditions and dynamics of mantle upwelling and melt extraction. For this goal to be achieved, our first-order understanding of mantle melting must be refined by high-quality, systematic data on correlated melt and residual phase compositions under known pressures and temperatures. Discrepancies in earlier data on melt compositions from a fertile mantle composition [MORB (mid-ocean ridge basalt) Pyrolite mg*-number 87] and refractory lherzolite (Tinaquillo Lherzolite* mg*-number 90) are resolved here. Errors in earlier data resulted from drift of W/Re thermocouples at 1 GPa and access of water, lowering liquidus temperatures by 30–80°C. We demonstrate the suitability of the 'sandwich' technique for determining the compositions of multiphase-saturated liquids in lherzolite, provided fine-grained sintered oxide mixes are used as the peridotite starting materials, and the changes in bulk composition are considered. Compositions of liquids in equilibrium with lherzolitic to harzburgitic residue at 1 GPa, 1300–1450°C in the two lherzolite compositions are reported. Melt compositions are olivine + hypersthene-normative (olivine tholeiites) with the more refractory composition producing a lower melt fraction (7–8% at 1300°C) compared with the model MORB source (18–20% at 1300°C).*

KEY WORDS: *mantle melting; sandwich experiments; reversal experiments; anhydrous peridotite melting; thermocouple oxidation; olivine geothermometry*

INTRODUCTION

The determination of peridotite partial melt compositions is an important constraint on models of magma genesis and geodynamics (Green & Falloon, 1998). However, the experimental determination of mantle melt compositions is not an easy matter (Falloon *et al.*, 1997, 1999*a*). One of the major hurdles facing any experimental study is quench modification of the melt composition by rapid metastable crystallization on the rims of primary crystal phases during quenching of the experimental run. One technique used extensively in experimental studies to avoid this problem is the so-called 'sandwich technique', wherein a layer of basalt (a melt component) is allowed to react with melt and residual phases produced from the peridotite composition of interest (Stolper, 1980; Takahashi & Kushiro, 1983; Fujii & Scarfe, 1985; Falloon & Green, 1987, 1988). The rationale of the sandwich technique is straightforward: if we have thermodynamic equilibrium, then we are free to vary the modal proportions (hence the bulk composition) of equilibrium phases without affecting their compositions. Therefore in the sandwich experiment, a layer of a melt component (of composition close to the anticipated equilibrium melt composition) is placed in contact with the peridotite of interest (wherein a greater modal percentage of the main melt-contributing reactants has been prepared) and

*Corresponding author. Telephone: +61-3-62262454. Fax +61-3-62232547. E-mail: trevor.falloon@utas.edu.au

allowed to react, providing large areas of melt at the end of the experiment that can be more easily analysed and, more importantly, are relatively unaffected by quench modification. Sandwich experiments are also an analogue of wall-rock reaction processes in the Earth's mantle (Kelemen *et al.*, 1992) and are more appropriately referred to as peridotite reaction experiments. Obviously, the success of the sandwich technique in establishing correct mantle melt compositions will depend on the choice of reactants used, the nature of the starting materials, the elimination of other potential experimental problems (e.g. temperature control, Fe loss, volatile content, etc.), and the achievement of equilibrium.

The deliberate placement of chemically different layers in the experimental charge obviously introduces the possibility of local chemical systems in which phase compositions may differ, and the total charge may not reach equilibrium.

An alternative approach by Kinzler & Grove (1991, 1992) (abbreviated to KG91 and KG92 hereafter) to the determination of liquid compositions saturated in peridotite residual phases avoided peridotitic compositions but instead used basaltic compositions in which relatively small proportions of liquidus phases were present at the pressures and temperatures of interest. The identification of liquids lying on olivine + orthopyroxene + clinopyroxene ± plagioclase cotectics (and thus possible melts from plagioclase lherzolite or lherzolite residues) was based on systems dominated by liquid rather than crystalline phases.

Several recent studies, using other experimental techniques (KG91; KG92; Hirose & Kushiro, 1993; Baker & Stolper, 1994; Kushiro, 1996), have criticized the 'sandwich' approach for determination of peridotite partial melt compositions. In comparison with their own peridotite melting data, Kinzler and Grove (KG91; KG92) noted that melt compositions from sandwich experiments performed by both Fujii & Scarfe (1985) (FS85) and Falloon & Green (1987) (FG87) at 1 GPa had the following anomalous features compared with other experimental data: (1) temperatures for equilibrium with a spinel lherzolite residue were too high; (2) the glass compositions from sandwich experiments had normative diopside contents that could not be explained by the KG92 melt model; (3) glass compositions from sandwich experiments were not multiply saturated in the stated residual mineralogy at the P and T of the experiment. These anomalous features were attributed by KG92 to lack of reaction between the melt layer and the peridotite layer, implying that the equilibrium state had not been achieved during the course of the experiment.

Accordingly, here we critically evaluate our earlier data and other studies, to derive a thoroughly checked dataset at 1 GPa. We present reversal experiments on two of the glass compositions considered anomalous by KG92 from the FG87 dataset. We also present additional direct melting experiments and new reaction experiments on the peridotite compositions MPY-87 and TQ-40 used in the FG87 study. In Appendix B, we present the phase compositions, including new glass analyses normalized to the international glass standard VG-2, and thus are able to demonstrate mass balance calculations for the earlier experiments (Falloon & Green, 1987, 1998) as well as our new experiments. Robinson *et al.* (1998) (RWB98) have also applied the sandwich technique to determine the compositions of mantle melts at 1·5 GPa, and this study provides a useful comparison.

Our new results demonstrate that the temperatures of equilibrium reported in FG87 (and a subset of FG88) are in error (correct temperatures are presented in Appendix A) and two glass compositions reported in FG87 are incorrect, i.e. not multiply saturated with the stated residual phases. The lack of equilibrium in the two experiments, however, was due to thermocouple drift and the failure of the layered charge to re-establish equilibrium in the time available. Our new data demonstrate that the sandwich technique, used in an appropriate manner, is indeed an effective method for determining the equilibrium compositions of peridotite partial melt compositions.

DISCUSSION OF EARLIER DATA

KG92 concluded that the invariant points (10^5 Pa to 6 GPa) defined in the simple system CaO–MgO–Al_2O_3–SiO_2 (CMAS) represent the maximum temperatures possible for the equilibria olivine + orthopyroxene + clinopyroxene + spinel/plagioclase + liquid, i.e. liquid in equilibrium with a lherzolite residue as opposed to harzburgite, wehrlite or dunite residue. At 1 GPa, this temperature is ~1322°C (Walter & Presnall, 1994), and KG92 noted that the data of FG87 predict T of equilibrium with a spinel lherzolite residue extending to 1400°C, well above the inferred maximum temperature defined by the CMAS system (see KG92, fig. 3). KG92 also noted that a subset of the FG87 and the FS85 dataset had anomalously high CaO and CaO/Al_2O_3 values and consequent high normative diopside (Di) contents in comparison with other preferred data. The identification of these problem data led KG92 to doubt the attainment of equilibrium in the sandwich technique, and to state that 'sandwich experiments do not provide reliable approximations of melt compositions saturated with the spinel-lherzolite assemblage'.

To further test these conclusions, KG91 and KG92 performed crystallization experiments on a suspect melt composition from both FS85 (composition no. 10, table 6, FS85) and FG87 (glass from run T-2113, FG87) datasets. If these two compositions are indeed equilibrium

liquids, then they should be liquid and multiply saturated with their stated residual phases at the experimental P and T (1310°C in the case of the FS85 composition and 1375°C in the case of the FG87 composition). The test for multiple saturation is that the liquid composition, when reacted with the residual mineralogy at the stated P and T, does not change its composition. If the melting process includes any reaction relationship, i.e. incongruent melting relationship of one or more phases, then the liquidus phase(s) of the equilibrium melt will not reproduce the residual phases. In the case of both the FS85 and the FG87 compositions, both were liquids at their stated P and T, consistent with equilibrium, but clinopyroxene alone was the liquidus phase in both compositions. As no reaction experiments were performed by KG91 and KG92, the significance of clinopyroxene crystallizing as the sole liquidus phase in these compositions is uncertain. However, KG91 found that the composition from FG87 first crystallized clinopyroxene at 1325°C, 50° below the conditions specified by FG87. The differences between the FG87 result (liquidus at 1375°C) and the KG91 result (liquidus at 1325°C) could be caused by H_2O in the experiments of KG91 or incorrect temperature measurement by FG87, using a W/Re thermocouple.

To test these possibilities, we have performed crystallization and reaction experiments on the T-2113 composition as well as on an additional composition from the dataset of FG87 (T-2140). We will use the results from these experiments to critically evaluate the previously published data of FG87,88 and the peridotite-sandwich technique. We also present additional experimental data at 1 GPa for peridotite compositions MPY-87 and TQ-40. These two compositions are, respectively, a composition for source lherzolite for mid-ocean ridge basalt (MORB) based on a primitive olivine tholeiite glass (DSDP-3-18) (Green *et al.*, 1979) and a refractory natural lherzolite (Tinaquillo Lherzolite, Green & Falloon, 1998). Both have been extensively studied in their subsolidus and melting behaviour.

EXPERIMENTAL AND ANALYTICAL TECHNIQUES

Experimental techniques

Starting compositions

All starting compositions used in the experimental study are presented in Table 1. The starting compositions (except for T-2113, synthetic starting material kindly provided by R. Kinzler) were prepared from a mixture of analytical grade oxides and carbonates (Ca, Na, K), ground under acetone in an agate mortar. This mixture was pelletized and sintered overnight (~16–20 h) at 950°C. An appropriate amount of synthetic fayalite was then added to the sintered mixes and the mixture was again ground under acetone, before storage in glass vials in a 110°C oven. The composition TQ-40 (Table 1) is a refractory lherzolite (minus 40 wt % $Fo_{91\cdot9}$) composition modelled on the natural Tinaquillo Lherzolite (Jaques & Green, 1980). The rationale for using olivine-depleted compositions in experimental studies was presented in FG87. The compositions 10/1300, 15/1350 and 5/1250 (Table 1) are calculated equilibrium partial melt compositions of Tinaquillo Lherzolite from the study of Jaques & Green (1980). The composition 95-1 (Table 1) is a synthetic composition modelled on the primitive back-arc basin glass composition 123 95-1 studied by Falloon *et al.* (1999*b*).

Run assemblies and temperature control

All experiments (Tables 2 and 3), except two runs (TFB-11 and TFB-12, Table 2, which were performed at the University of Bristol), were performed using standard piston-cylinder techniques in the High Pressure Laboratory housed in the School of Earth Sciences, University of Tasmania (UTas). All experiments used NaCl–Pyrex assemblies (except runs T-3629 and T-3635, Table 2, which used talc–Pyrex assemblies) with graphite heaters and a $W_{97}Re_3/W_{75}Re_{25}$ (W/Re, Type D) thermocouple (calibrated against the melting point of Au and the e.m.f. of a Type S, $Pt/Pt_{90}Rh_{10}$ (Pt) thermocouple, at atmospheric P in an Ar atmosphere). Temperatures were controlled to within ± 1°C of the set point using a Eurotherm type 818 controller. No P correction was applied to the thermocouple calibration. All UTas experiments employed graphite capsules with fired pyrophyllite and alumina spacers, and mullite and alumina surrounds. The thermocouple enters the assembly through a composite two- and four-bore alumina sheath and is shielded from the graphite capsule by a 1 mm alumina disc. The thermocouple junction is formed by crossing the thermocouple wires utilizing the four-bore alumina sheath, which forms the top 5 mm of the alumina thermocouple sheath. All experimental components and starting materials were stored in an oven at 110°C. Experiments were performed using the hot piston-out technique (Johannes *et al.*, 1971). For experiments with run numbers >T-4276, an initial overpressurization of ~0·5 GPa was employed to help prevent oxidation of the W/Re thermocouple. In our more recent work (Falloon *et al.*, in preparation) we employ a continuous nitrogen gas flow over the thermocouple exit from the end plate of the piston-cylinder apparatus, which prevents thermocouple oxidation at 1 GPa (Walter & Presnall, 1994). The overpressurization technique employed in this study produces results consistent with this new work at 1 GPa. Pressures are accurate to within $\pm 0\cdot1$ GPa.

Table 1: Starting compositions used in this study

Composition	SiO_2	TiO_2	Al_2O_3	Cr_2O_3	FeO	MnO	MgO	CaO	Na_2O
T-2113	50·47	0·42	15·29	0·32	7·41		12·05	12·83	1·15
T-2140	50·78	0·67	15·42	0·27	7·79		11·12	12·10	1·83
MPY-87	44·32	0·16	4·33	0·44	9·82	0·10	36·84	3·34	0·39
TQ-40	47·50	0·13	5·35	0·75	7·51	0·18	32·80	4·97	0·30
TQ	44·95	0·08	3·22	0·45	7·66	0·14	40·03	2·99	0·18
10/1300	49·03	0·30	14·35		9·00		13·63	12·40	1·15
15/1350	47·12	0·53	14·47		10·93		14·57	10·88	1·25
5/1250	50·09	0·33	17·86		7·68		10·20	12·44	1·30
95-1	47·90	0·42	16·52	0·11	8·49	0·11	10·67	14·30	1·40

High-pressure experiments performed at the University of Bristol (UB) used $BaCO_3$ pressure cells with a graphite furnace, and $BaCO_3$ and crushable alumina as inner spacers. Starting compositions were loaded into inner graphite capsules and sealed into an outside platinum capsule (3 mm o.d.) by welding. Experiments used a W/Re thermocouple entering the assembly through a four-bore alumina sleeve. The thermocouple was protected from the capsule by a thin alumina disc (1 mm). No *P* correction was applied to the thermocouple calibration. Experiments were brought to the desired *P* and *T* using the hot piston-out technique.

Analytical techniques

Electron microprobe microanalysis

At the end of each experiment, the entire experimental charge was mounted and sectioned longitudinally before polishing. Experimental phase compositions presented in Table 4 were analysed either by wavelength-dispersive microanalysis using a Cameca SX-50 microprobe housed in the Central Science Laboratory, UTas (operating conditions 15 keV, 20–25 ηA) or energy-dispersive microanalysis using a Cameca MICROBEAM microprobe housed in the Research School of Earth Sciences, The Australian National University (operating conditions 15 keV, 5 ηA). All glass analyses have been normalized to the composition of international glass standard VG-2 (Jarosewich *et al.*, 1980), which was analysed together with the glasses under the same analytical conditions.

Phase compositions for the FG87,88 experiments are presented in Appendix B. The phase compositions were analysed by either wavelength- or energy-dispersive microanalysis. Wavelength-dispersive microanalysis was performed using either the UTas SX-50 microprobe or a Jeol JXA 8600 Superprobe with Link Analytical AN10/85S X-ray analysis system and LEMAS automation, housed in the Department of Geology, UB (operating conditions 15 keV, 15 ηA). Energy-dispersive microanalysis was performed by a JEOL JX-50A electron probe microanalyser (operating conditions 15 keV, 5 ηA, calibrated using pure Cu, formerly housed in the Central Science Laboratory, UTas). Reanalysed glass analyses, normalized to VG-2, were performed using wavelength-dispersive microanalysis using the UTas SX-50 microprobe.

FTIR spectroscopy

H_2O contents of selected experimental glasses (Table 5), including some from the study of FG87,88, were determined using Fourier transform infrared (FTIR) spectroscopy. Measurements were performed using a Bruker IFS 66 spectrometer with attached optical microscope (all reflecting optics) and Bruker Opus/IR reduction software, housed in the Central Science Laboratory, UTas. Run products were doubly polished (30–70 μm thick, using superglue for bonding to a standard thin-section glass slide, during polishing). Diameters of analysed areas were usually 60–90 μm. During each analysis, 100 scans were collected with the resolution of four wavenumbers between 4000 and 2400 cm^{-1}. H_2O contents were estimated using the main OH-stretching peak at $\sim$3500 cm^{-1} following the calibration of Danyushevsky *et al.* (1993).

*Calculation of %*F *in peridotite melting and reaction experiments*

To calculate the degree of partial melting (%*F*) for the peridotite compositions of interest in this study (Tinaquillo Lherzolite and MORB Pyrolite) we have applied the following procedures to our direct melting and reaction experiments on the TQ-40 and MPY-87 compositions.

Table 2: Experimental run data on T-2113 (inferred melt), TQ-40 and (T-2113 + TQ-40) compositions

No.	Run no.	Run *T* (°C)	Calculated *T* (°C)	Time (h, min)	Wt % basalt	ML_i/ML_f	Basalt composition	Phase assemblage
Crystallization experiments (T-2113)								
1	T-4123	1375		24			T-2113	L
2	T-4313	1350		27, 10			T-2113	L
3	T-4320	1340		24, 20			T-2113	L
4	T-4300	1325		25, 30			T-2113	Cpx + L
Peridotite reaction and melting experiments								
Series D								
5	T-3629	1375	1370	3	17·9	0·371	10/1300	Ol + Opx + L
6	T-3635	1325	1319	3	24·6		10/1300	Ol + Opx + Cpx + Sp + L
7	T-4081	(i) 1500		1				
		(ii) 1375	1381	24	0			Ol + Opx + L
8	T-4126	(i) 1500		1				
		(ii) 1325	1314	24	0			Ol + Opx + Cpx + Sp + L
Series E								
9	T-3980	1325	1310	24	12·0	0·380	5/1250	Ol + Opx + Cpx + Sp + L
10	T-3981	1325	1321	24	15·4	0·440	15/1350	Ol + Opx + Cpx + Sp + L
11	T-4125	1375	1325	24	38·0	0·718	T-2113	Ol + Opx + Cpx + Sp + L
12	TFB-11	1314	1380	24	16·5	0·337	15/1350	Ol + Opx + L
13	TFB-12	1314	1371	5	18·4	0·376	5/1250	Ol + Opx + L
14	T-4080	1375	1344	24, 10	40·0	0·727	95–1	Ol + Opx + L
15	T-4321	1325	1359	97, 7	25·0	0·535	T-2113	Ol + Opx + L
16	T-3982	1325		24	0			Ol + Opx + Cpx + Sp + L
17	T-3976	1350	1349	29, 10	0			Ol + Opx + Cpx + Sp + L
18	T-3978	1400		24, 15	0			Ol + Opx + Sp + L
19	T-4304	1400	1409	21, 30	0			Ol + Opx + L
20	T-4014	1450	1411	24	0			Ol + Opx + L
21	T-4301	1450	1495	25, 10	0			Ol + L
22	T-4174	1500		1	0			Ol + L

ML_i/ML_f, ratio of the initial mass of liquid in the bulk composition (given by wt % basalt) and the final mass of liquid in the bulk composition (given by mass balance, Table 4). Ol, olivine; opx, orthopyroxene; cpx, clinopyroxene; sp, spinel; L, glass. Calculated temperature (°C) is the calculated OLT using the Ford *et al.* (1983) geothermometer.

(1) For each experiment we first use the known bulk composition of the experiment to test for mass balance of all residual phases using least-squares linear regression (using the software Petmix). If the experiment has come to equilibrium and all phases have been analysed correctly then we must be able to demonstrate positive proportions for all phases with a very low sum of the squares of the residuals for the oxides. In the case of our direct melting and reaction experiments ($n = 23$) were are able to demonstrate positive proportions for all phases with very low sum of the squares of the residuals (average 0·08 $\pm$ 0·07, range 0·0023–0·2968; see Tables 4 and 6). In general, if an experiment as a result of a least-squares linear regression mass balance calculation has negative phase proportions and/or a very high sum of the squares of the residuals (i.e. $\gg 1{\cdot}0$), then there is either a problem with attainment of equilibrium over the course of the experiment or alternatively there are significant errors in the analyses of the experimental phases, and/or calculation of the bulk composition (i.e. error or inaccuracy in the weighing in of the layered components so that the nominal bulk composition differs from the true bulk composition). Such experiments should not be used for any petrogenetic modelling.

In the case of direct melting experiments this is all that is necessary to calculate the %*F* present in the experiment. The %*F* calculated for direct melting experiments on the TQ-40 and MPY-87 compositions by mass balance is

Table 3: Experimental run data on T-2140 (inferred melt), MPY and (T-2140 + MPY-87) compositions

No.	Run no.	Run *T* (°C)	Calculated *T* (°C)	Time (h, min)	Wt % basalt	ML_i/ML_f	Basalt composition	Phase assemblage
Crystallization experiments (T-2140)								
1	T-4090	1400		24			T-2140	L
2	T-4282	1350		26			T-2140	L
3	T-4283	1338		24, 15			T-2140	Cpx + L
4	T-4276	1320		21			T-2140	Cpx + L
Peridotite reaction and melting experiments								
Series D								
5	T-4083	1400	1391	24	77·0	0·816	T-2140	Ol + L
6	T-4324	1320	1325	72, 25	12·7	0·397	T-2140	Ol + Opx + Cpx + Sp + L
7	T-4296	1338	1336	67, 30	33·0	0·660	T-2140	Ol + Opx + L
Series E								
8	T-4338	1319	1330	46	35·0	0·648	T-2140	Ol + Opx + L
9	T-4284	1344	1349	75, 40	12·7	0·363	T-2140	Ol + Opx + Sp + L
10	T-4318	1330	1355	73	13·2	0·363	T-2140	Ol + Opx + L
11	T-4183	1400	1363	26	16·0	0·381	T-2140	Ol + Opx + L
12	T-4033	1300		24	0			Ol + Opx + Cpx + Sp + L
13	T-4297	1337	1328	49	0			Ol + Opx + L
14	T-4298	1400	1371	45, 30	0			Ol + Opx + L
15	T-4306	1450	1441	21, 15	0			Ol + L

ML_i/ML_f, ratio of the initial mass of liquid in the bulk composition (given by wt % basalt) and the final mass of liquid in the bulk composition (given by mass balance, Table 4). Ol, olivine; opx, orthopyroxene; cpx, clinopyroxene; sp, spinel; L, glass. Calculated temperature (°C) is the calculated OLT using the Ford *et al.* (1983) geothermometer.

given in Table 6 (column 4). RWB98 proposed a more sophisticated method of calculating %*F*, by calculating *F* and its standard error for each individual oxide resulting in a calculation of an average %*F* as a weighted mean with a standard error (see their appendix). Figure 1 and Table 6 demonstrates that simple mass balance for all oxides by linear least-squares regression (where the calculation demonstrates positive phase proportions and a very low sum of the squares of the residuals) produces identical results to the RWB98 calculation. In the calculation of %*F* by the method of RWB98 the phase proportions of spinel used were those given by mass balance, not an arbitrary small amount of 0·2 wt % as proposed by RWB98.

To calculate the %*F* for the TQ (Table 1) composition we simply multiply column 7, Table 6, by 0·6, as the only difference between the TQ-40 and TQ compositions is the subtraction of 40 wt % olivine, and these values are given in column 9, Table 6.

(2) In the case of peridotite reaction experiments the next step is to test for mass balance into the peridotite of interest using the analysed melt and phases in the reaction experiment. There should be positive proportions for all phases and a very low sum of the squares of the residuals. In all cases ($n = 14$) we are able to demonstrate positive proportions for all phases with very low sum of the squares of the residuals (average for TQ-40 reaction experiments $0{\cdot}15 \pm 0{\cdot}14$, $n = 8$, range 0·0219–0·4753; average for MPY-87 reaction experiments $0{\cdot}05 \pm 0{\cdot}04$, $n = 6$, range 0·0055–0·1143; see Tables 4 and 6). The residual sums for reaction experiments on TQ-40 are higher than for the MPY-87 reaction experiments because the reactants used were significantly different in composition from the expected equilibrium partial melt, except for runs T-4125 and T-4321, which have residuals similar to those of the MPY-87 reaction experiments (Table 6). We also calculated the %*F* into the peridotite of interest using the method of RWB98 and again found identical results to our mass balance calculations (Table 6), i.e. both methods are 'correct' if applied to equilibrium experiments in which the added melt layer does not diverge strongly from the equilibrium melt composition.

(3) The final step in establishing the %*F* of the peridotite of interest from our reaction experiments is to compare the compositions and mode of residual crystals in the reaction experiments with those in direct experiments on the peridotite of interest at the same *P* and *T*. We have

Table 4: Compositions of experimental run products

Run no.	Phase	MB	Type	SiO_2	TiO_2	Al_2O_3	FeO	MnO	MgO	CaO	Na_2O	Cr_2O_3	NiO	Probe
Crystallization experiments on T-2113														
T-4300	Clinopyroxene	0·26(2)	A(3)	51·2(2)	0·17(0)	7·3(4)	5·8(1)		19·6(6)	14·4(5)	0·32(5)	1·1(1)		100·9(2)
	Glass	0·73(2)	A(3)	51·4(1)	0·56(3)	17·71(8)	7·66(7)		8·85(4)	12·18(6)	1·43(3)	0·18(2)		101·0(2)
	Residual	**0·7354**												
Peridotite reaction and melting experiments on TQ-40														
Series D														
T-3629	Olivine	0·361(3)	A(5)	40·8(1)			9·2(1)	0·15(3)	48·8(1)	0·36(4)		0·41(1)	0·27(7)	101·2(2)
	Orthopyroxene	0·154(6)	A(5)	55·5(4)	0·06(4)	2·7(6)	5·6(1)	0·15(2)	32·4(5)	2·3(2)	0·03(1)	1·2(2)	0·12(4)	101·13(7)
	Glass	0·483(4)	A(5)	50·8(1)	0·33(3)	13·6(1)	7·6(2)	0·19(2)	14·00(5)	11·9(2)	0·96(4)	0·51(4)	0·02(1)	100·6(4)
	Residual	**0·0130**												
T-3635	Olivine		A(7)	41·4(8)			10·3(2)	0·16(4)	47·3(7)	0·37(5)			0·47(5)	101·7(1)
	Orthopyroxene		A(6)	54·0(2)	0·07(2)	4·8(2)	6·1(1)	0·19(4)	30·7(3)	2·65(8)	0·05(2)	1·45(9)		101·4(4)
	Clinoproxene		n.d.											
	Spinel		n.d.											
	Glass		A(5)	50·2(1)	0·40(3)	15·49(7)	7·6(1)	0·19(3)	11·64(5)	12·86(6)	1·24(2)	0·26(1)	0·05(5)	101·3(2)
T-4081	Olivine	0·409(6)	A(3)	41·2(1)			8·6(1)		49·91(8)	0·15(5)		0·26(4)		100·98(6)
	Orthopyroxene	0·227(9)	A(2)	55·9(2)		2·5(2)	5·18(0)		33·3(3)	1·84(5)		1·33(5)		100·1(9)
	Glass	0·355(6)	A(5)	50·5(1)	0·43(2)	13·32(2)	7·6(1)	0·16(3)	13·62(6)	12·9(1)	0·87(3)	0·56(7)		99·2(3)
	Residual	**0·0456**												
T-4126	Olivine	0·393(2)	A(2)	40·53(4)			9·4(1)	0·2(1)	49·0(3)	0·32(6)			0·51(7)	99·4(1)
	Orthopyroxene	0·276(4)	A(4)	54·5(8)	0·09(1)	3·9(9)	5·8(2)	0·19(9)	31·6(6)	2·70(5)	0·08(1)	1·3(3)		98·6(3)
	Clinoproxene	0·077(5)	A(3)	53·0(1)	0·11(2)	4·5(2)	5·1(1)	0·20(8)	24·7(5)	10·9(5)	0·16(2)	1·5(1)		99·5(1)
	Spinel	tr.	S			35·39	9·87		18·39	0·08		36·27		102·14
	Glass	0·249(3)	A(6)	50·0(1)	0·54(3)	15·8(1)	7·3(9)	0·15(5)	11·62(6)	13·1(1)	1·18(6)	0·38(4)		99·8(3)
	Residual	**0·0023**												
Series E														
T-3980	Olivine	0·329(5)	A(4)	40·32(6)			9·6(1)	0·19(6)	48·8(2)	0·4(1)		0·24(3)	0·46(6)	100·1(5)
	Orthopyroxene	0·286(9)	A(3)	54·2(5)	0·06(0)	4·3(5)	5·66(3)	0·19(2)	31·6(2)	2·68(4)	0·04(1)	1·3(1)		99·8(7)
	Clinoproxene	0·066(8)	Sel	51·67	0·16	5·62	4·45	0·16	21·82	14·34	0·22	1·56		100·25
	Spinel		n.d.											
	Glass	0·316(6)	A(5)	49·52(6)	0·48(2)	16·8(1)	7·42(8)	0·16(4)	11·3(1)	12·79(4)	1·36(3)	0·23(3)		100·0(4)
	Residual	**0·0195**												
T-3981	Olivine	0·350(2)	A(5)	40·2(2)			10·19(1)	0·20(3)	48·4(2)	0·36(2)		0·25(5)	0·44(2)	99·9(6)
	Orthopyroxene	0·262(4)	A(6)	54·1(3)	0·09(1)	4·2(4)	5·9(3)	0·21(5)	31·3(2)	2·9(1)	0·04(2)	1·32(7)		99·9(8)
	Clinoproxene	0·034(3)	A(3)	51·8(4)	0·17(2)	5·1(6)	4·6(2)	0·19(4)	21·5(9)	14·9(9)	0·21(4)	1·58(8)		99·7(5)
	Spinel		n.d.											
	Glass	0·350(3)	A(5)	49·8(1)	0·55(3)	15·53(7)	8·0(1)	0·14(4)	11·7(1)	12·78(8)	1·28(3)	0·29(5)		100·0(2)
	Residual	**0·0032**												

Table 4: continued

Run no.	Phase	MB	Type	SiO_2	TiO_2	Al_2O_3	FeO	MnO	MgO	CaO	Na_2O	Cr_2O_3	NiO	Probe
T-4125	Olivine	0·223(3)	A(5)	40·85(9)			9·8(1)		49·11(6)	0·15(3)		0·14(4)		99·3(7)
	Orthopyroxene	0·213(5)	A(5)	55·2(6)		3·3(7)	5·6(2)		32·7(5)	2·0(2)		1·3(1)		99·3(4)
	Clinoproxene	0·029(4)	Sel	52·5		5·19	4·12		21·28	15·45		1·45		98·3
	Spinel		n.d.											
	Glass	0·529(4)	A(5)	49·90(9)	0·48(3)	15·32(6)	7·62(6)	0·09(3)	12·00(7)	13·08(8)	1·16(4)	0·35(3)		100·8(3)
	Residual	**0·0063**												
TFB-11	Olivine	0·37(1)	A(5)	41·05(8)			8·7(3)	0·18(3)	49·8(2)	0·32(2)			0·03(3)	100·2(3)
	Orthopyroxene	0·13(2)	A(5)	54·9(2)	0·05(2)	3·5(4)	5·4(1)	0·13(5)	32·2(3)	2·19(8)	0·06(4)	1·56(8)		100·2(4)
	Glass	0·49(1)	A(5)	50·8(1)	0·47(1)	12·86(5)	7·9(1)	0·14(6)	14·3(1)	11·7(1)	0·99(2)	0·38(2)		97·6(4)
	Residual	**0·1840**												
TFB-12	Olivine	0·316(8)	A(4)	41·0(1)			8·5(2)	0·17(6)	49·9(1)	0·30(2)			0·12(6)	99·9(3)
	Orthopyroxene	0·19(1)	A(5)	55·2(3)	0·07(3)	3·8(5)	5·4(1)	0·15(6)	32·0(3)	2·1(1)		1·27(3)		100·3(5)
	Glass	0·49(1)	A(6)	50·18(9)	0·36(2)	14·42(6)	7·44(6)	0·21(4)	13·96(7)	11·86(4)	1·06(3)	0·37(3)		97·8(2)
	Residual	**0·0917**												
T-4080	Olivine	0·277(5)	A(3)	41·0(1)			9·1(1)		49·60(7)	0·14(2)		0·19(1)		100·7(4)
	Orthopyroxene	0·047(7)	S	56·26		2·75	4·67		33·41	1·98		0·94		98·6
	Glass	0·671(5)	A(5)	50·1(3)	0·41(3)	14·4(3)	7·5(1)	0·17(2)	12·9(1)	12·92(7)	1·08(3)	0·53(4)		100·6(3)
	Residual	**0·0302**												
T-4321	Olivine	0·269(2)	A(4)	40·5(1)			9·3(2)	0·08(2)	49·2(3)	0·33(2)		0·38(4)	0·20(1)	101·4(5)
	Orthopyroxene	0·261(3)	A(3)	54·4(2)	0·06(3)	4·0(1)	5·6(1)	0·13(4)	31·6(3)	2·6(2)	0·04(2)	1·49(1)	0·15(7)	101·4(3)
	Glass	0·467(2)	A(5)	49·84(8)	0·47(2)	14·37(8)	7·6(1)	0·14(4)	13·2(1)	13·0(1)	0·96(3)	0·42(7)		101·6(4)
	Residual	**0·0046**												
T-3982	Olivine		A(6)	40·4(2)			9·3(2)	0·21(3)	48·92(9)	0·33(3)		0·25(3)	0·63(2)	100·9(2)
	Orthopyroxene		A(2)	54·2(4)	0·08(1)	4·2(4)	5·61(7)	0·16(2)	31·7(2)	2·8(2)	0·04(2)	1·35(0)		100·7(4)
	Clinoproxene		Sel	52·28	0·12	4·59	4·26	0·18	21·82	14·92	0·20	1·62		100·42
	Spinel		n.d.											
	Glass		n.d.											
T-3976	Olivine	0·406(4)	A(5)	40·5(3)			8·7(3)	0·19(3)	49·2(4)	0·38(9)		0·35(3)	0·65(6)	100·6(5)
	Orthopyroxene	0·271(9)	A(3)	54·5(5)		4·1(6)	5·8(2)	0·2(1)	31·1(6)	2·5(1)		1·8(2)		97·8(5)
	Clinoproxene	0·02(1)	A(4)	53·1(4)	0·11(3)	4·3(2)	5·2(3)	0·20(6)	24·7(3)	10·6(7)	0·15(2)	1·68(9)		99·8(7)
	Spinel		n.d.											
	Glass	0·305(6)	A(5)	50·4(1)	0·48(2)	13·8(4)	7·4(2)	0·19(5)	13·1(7)	13·0(3)	1·04(4)	0·55(7)		100·2(6)
	Residual	**0·0126**												
T-3978	Olivine		A(3)	40·5(2)			8·4(2)	0·15(4)	49·73(2)	0·36(4)		0·36(6)	0·54(1)	100·87(9)
	Orthopyroxene		A(2)	56·4(5)		2·0(4)	5·03(6)	0·17(3)	33·6(1)	1·78(8)		1·03(8)		99·6(6)
	Spinel		A(3)	0·4(2)	0·23(8)	25·1(2)	10·1(2)	0·23(8)	17·0(3)	0·24(3)		46·8(3)		98(4)
	Glass		n.d.											
T-4304	Olivine	0·430(7)	A(4)	41·6(1)			8·28(4)		49·4(2)	0·32(2)		0·46(5)		100·2(5)
	Orthopyroxene	0·16(1)	A(5)	56·1(5)		2·6(7)	5·4(1)		32·0(5)	2·8(1)		1·1(1)		99·8(5)
	Glass	0·405(8)	A(3)	51·3(2)	0·34(6)	11·81(6)	7·9(1)		16·05(7)	11·09(7)	0·79(6)	0·72(6)		99·7(4)
	Residual	**0·0532**												

Run no.	Phase	MB	Type	SiO_2	TiO_2	Al_2O_3	FeO	MnO	MgO	CaO	Na_2O	Cr_2O_3	NiO	Probe
T-4014	Olivine	0·427(8)	A(5)	40·9(2)			7·7(1)	0·17(2)	50·2(2)	0·17(4)		0·36(6)	0·6(2)	100·8(7)
	Orthopyroxene	0·12(1)	A(4)	57·2(4)		1·4(5)	4·5(1)	0·12(8)	34·5(5)	1·4(2)		1·4(5)		99(2)
	Glass	0·450(9)	A(5)	51·7(2)	0·33(3)	11·7(1)	7·6(2)	0·20(6)	16·3(2)	10·7(2)	0·77(3)	0·80(9)		100·8(7)
	Residual	**0·0963**												
T-4301	Olivine	0·394(3)	A(5)	41·8(1)			6·72(5)		50·8(1)	0·21(2)		0·47(4)		99·6(7)
	Glass	0·598(3)	A(5)	52·1(1)	0·28(4)	8·6(1)	7·9(1)	0·07(7)	21·4(1)	8·2(1)	0·5(1)	0·97(7)		100·2(4)
	Residual	**0·0747**												
T-4174	Olivine		A(3)	41·19(9)			6·31(8)	0·15(1)	51·2(2)	0·23(4)		0·39(6)	0·56(9)	99·3(5)
Crystallization experiments on T-2140														
T-4283	Clinopyroxene	0·05(1)	A(7)	52·9(5)	0·16(5)	4·6(4)	5·0(3)		20·9(8)	15·1(9)	0·32(6)	1·1(1)		101·5(4)
	Glass	0·95(1)	A(6)	50·7(2)	0·68(4)	15·8(2)	8·0(1)		10·3(1)	12·34(6)	1·86(6)	0·25(4)		101·5(6)
	Residual	**0·2667**												
T-4276	Clinopyroxene	0·15(1)	A(5)	52·3(1)	0·21(6)	5·5(3)	5·3(3)		19·9(6)	16(1)	0·26(8)	1·0(1)		100·5(5)
	Glass	0·84(1)	A(10)	50·6(2)	0·73(7)	17·1(3)	8·37(7)		9·2(2)	11·80(7)	2·05(9)	0·15(8)		101·2(9)
	Residual	**0·2202**												
Peridotite melting and reaction experiments on MPY-87														
Series D														
T-4083	Olivine	0·052(6)	A(3)	41·11(6)			8·7(3)		50·1(3)	0·06(5)				101·2(6)
	Glass	0·943(7)	A(5)	49·8(1)	0·54(1)	14·5(2)	8·2(1)		14·67(6)	10·6(1)	1·37(6)	0·32(6)		99·8(3)
	Residual	**0·3845**												
T-4324	Olivine	0·504(6)	A(6)	40·1(2)			11·4(1)	0·13(2)	47·5(3)	0·32(1)		0·24(4)	0·24(5)	102·0(5)
	Orthopyroxene	0·16(1)	A(5)	53·1(3)	0·13(2)	5·3(2)	6·9(1)	0·07(5)	30·4(2)	2·6(2)	0·08(1)	1·3(1)	0·10(3)	102·0(5)
	Clinopyroxene	0·018(9)	A(3)	51·5(5)	0·24(2)	6·1(6)	5·1(2)	0·10(4)	20·5(2)	14·9(3)	0·35(2)	1·6(1)		101·74(6)
	Spinel	0·00(2)	A(3)	0·20(1)	0·22(2)	44(1)	10·9(2)	0·04(6)	18·4(3)	0·11(2)		26(1)		102·4(3)
	Glass	0·32(1)	A(5)	49·2(3)	0·79(1)	15·90(5)	8·41(3)	0·10(8)	11·60(7)	12·1(1)	1·65(2)	0·30(3)		101·4(3)
	Residual	**0·0165**												
T-4296	Olivine	0·40(1)	A(5)	40·74(7)			11·07(9)		47·6(1)	0·37(3)		0·23(6)		100·8(2)
	Orthopyroxene	0·10(2)	A(3)	55·0(2)		3·8(2)	6·51(8)		30·67(2)	2·8(1)		1·22(6)		100·8(6)
	Glass	0·50(1)	A(4)	49·62(9)	0·66(5)	15·00(6)	8·6(1)		12·06(8)	12·25(9)	1·56(9)	0·29(4)		100·6(3)
	Residual	**0·1709**												
Series E														
T-4338	Olivine	0·410(9)	A(5)	40·4(2)			10·8(2)	0·06(3)	47·7(2)	0·33(2)		0·33(2)	0·23(4)	100·0(2)
	Orthopyroxene	0·05(1)	A(6)	54·7(5)	0·09(2)	3·7(7)	6·5(2)	0·10(3)	31·1(4)	2·6(2)	0·07(1)	1·1(1)	0·09(4)	100·4(5)
	Glass	0·54(1)	A(5)	49·8(1)	0·68(1)	15·07(7)	8·5(1)	0·09(2)	11·71(5)	12·1(2)	1·74(3)	0·31(2)	0·02(2)	100·2(3)
	Residual	**0·0921**												
T-4284	Olivine	0·54(1)	A(4)	40·8(2)			10·85(8)		47·8(2)	0·31(4)		0·29(2)		99·0(4)
	Orthopyroxene	0·10(2)	A(4)	54·6(3)	0·02(5)	3·8(5)	6·6(3)		31·1(5)	2·5(3)		1·39(9)		99·5(8)
	Spinel	0·004(4)	A(2)		0·33(2)	34·7(3)	11·3(2)		17·5(2)	0·12(4)		36·1(3)		102·4(8)
	Glass	0·35(1)	A(7)	49·7(2)	0·73(6)	14·3(1)	9·0(1)		12·7(1)	11·8(1)	1·41(6)	0·37(4)		100·2(3)
	Residual	**0·1164**												

Table 4: continued

Run no.	Phase	MB	Type	SiO_2	TiO_2	Al_2O_3	FeO	MnO	MgO	CaO	Na_2O	Cr_2O_3	NiO	Probe
T-4318	Olivine	0·528(9)	A(5)	40·3(2)			11·0(2)	0·12(1)	47·7(2)	0·32(2)		0·36(6)	0·19(2)	100·1(4)
	Orthopyroxene	0·11(1)	A(5)	54·8(5)	0·08(4)	3·6(2)	6·7(1)	0·11(2)	31·3(4)	2·2(1)	0·05(0)	1·14(9)	0·05(5)	101·3(6)
	Glass	0·364(9)	A(5)	49·4(1)	0·69(2)	14·5(1)	8·9(1)	0·13(3)	13·03(9)	11·5(1)	1·34(2)	0·40(5)		100·3(3)
	Residual	**0·0897**												
T-4183	Olivine	0·53(1)	A(4)	40·38(8)			10·7(1)	0·12(4)	48·0(2)	0·28(4)		0·38(4)	0·12(2)	99·5(5)
	Orthopyroxene	0·04(2)	A(2)	55·4(4)	0·11(0)	2·95(5)	6·3(1)	0·08(5)	32·3(3)	1·91(1)	0·05(0)	0·81(1)		99·46(7)
	Glass	0·42(1)	A(5)	50·7(2)	0·52(1)	13·79(3)	9·0(1)	0·13(3)	13·28(7)	10·79(8)	1·45(2)	0·43(6)		98·3(4)
	Residual	**0·1198**												
T-4033	Olivine		A(4)	40·2(1)			11·8(1)	0·13(9)	47·5(1)	0·18(2)			0·2(2)	101·4(3)
	Orthopyroxene		A(4)	53·1(4)	0·23(5)	6·4(6)	7·1(1)	0·13(9)	29·7(2)	2·5(4)		0·94(4)		99·4(2)
	Clinoproxene		A(3)	51·3(2)	0·45(9)	6·9(9)	4·73(4)	0·04(7)	18·5(7)	16·7(2)	0·2(1)	1·1(2)		99·3(6)
	Spinel		A(5)	0·5(2)	0·25(3)	46(2)	10·6(2)		18·0(3)	0·04(5)		25(2)		103·8(2)
	Glass		n.d.											
T-4297	Olivine	0·64(2)	A(5)	40·7(2)			11·3(2)		47·2(2)	0·36(9)		0·35(2)		101(1)
	Orthopyroxene	0·12(3)	A(3)	54·9(3)	0·14(4)	4·1(2)	6·9(1)		30·4(3)	2·6(2)		1·13(4)		101·0(6)
	Glass	0·23(2)	A(5)	49·3(2)	0·82(5)	14·8(2)	9·0(1)		11·8(1)	12·3(1)	1·4(1)	0·40(4)		100·6(7)
	Residual	**0·2968**												
T-4298	Olivine	0·641(6)	A(5)	40·9(1)			10·7(1)		47·76(2)	0·25(3)		0·35(3)		101(1)
	Orthopyroxene	0·08(1)	A(3)	54·6(3)	0·07(6)	4·3(7)	6·5(1)	0·04(7)	30·7(6)	2·3(4)		1·44(4)		102·0(5)
	Glass	0·280(7)	A(10)	49·8(1)	0·70(5)	13·9(1)	9·3(2)		13·7(3)	10·7(2)	1·3(1)	0·48(5)		102·4(8)
	Residual	**0·0367**												
T-4306	Olivine	0·625(2)	A(5)	41·1(2)			9·8(1)		48·5(1)	0·24(2)		0·35(6)		100·7(7)
	Glass	0·373(2)	A(6)	50·0(4)	0·53(3)	11·4(4)	10·3(4)		17·4(4)	8·5(3)	1·1(1)	0·58(3)	0·05(3)	100·4(6)
	Residual	**0·0313**												

Numbers in parentheses next to each analysis or mass balance are 1σ in terms of the last units cited; e.g. 0·540(9) refers to 0·540$\pm$0·009. Mass balance (MB) in weight fraction was performed using least-squares linear regression using the software Petmix, and 'Residual' refers to the sum of the squares of the residuals. All analyses have been normalized to 100 wt % before averages have been calculated; the average unnormalized totals are given under 'Probe'. 'Type' refers to whether the analysis is an average (A), with the number used to form the average given in parentheses; 'Sel' refers to a selected analysis in those cases (commonly clinopyroxene) where either the small size of the crystal or its form (e.g. thin tabular laths) caused analyses to have significant overlaps with other phases; 'S' refers to a single analysis in those cases where only one analysis was obtained; 'n.d.' refers to not determined, either because the glass phase was quench modified or because the very small grain size (especially spinel) made analysis without significant overlaps impossible; tr., trace.

Table 5: H_2O contents of 'nominally anhydrous' experimental glasses

Run no.	*T* (°C)	Anhydrous *T* (°C)	%H_2O	Hydrous *T* (°C)
Falloon & Green (1987), Series A				
T-1511	1220	1277	0·50	1219
T-1478	1225	1322	0·44	1266
T-1480	1275	1367	0·69	1302
Falloon & Green (1987), Series B				
T-2113	1375	1327	0·08	1296
T-2138	1350	1299	0·08	1268
Peridotite melting experiments				
T-4301	1450	1496	0·10	1461
Crystallization experiments				
T-4320 (T-2113)	1340	—	0·06	—
T-4300 (T-2113)	1325	—	0·05	—
T-4282 (T-2140)	1350	—	0·07	—
T-4283 (T-2140)	1338	—	0·07	—
Peridotite reaction experiments				
T-3629	1375	1370	0·04	—
T-3980	1325	1310	0·15	—
T-3981	1325	1321	0·15	—
TFB-11	1314	1380	0·65	1316
TFB-12	1314	1371	0·66	1307
T-4284	1344	1349	0·14	—
T-4318	1330	1355	0·04	1331

Temperature (°C) is the nominal run temperature. Anhydrous temperature (°C) is the OLT calculated using the olivine geothermometer of Ford *et al.* (1983). Hydrous temperature (°C) is calculated using the empirical expression of Falloon & Danyushevsky (2000).

made this comparison in two ways. First, we have used the method of RWB98 to demonstrate that there is no significant difference between calculated %*F* when using either the proportions of solid phases in the actual bulk composition or those calculated by mass balance for the peridotite of interest (compare columns 6 and 7, Table 6). The close matching of these results demonstrates that the addition of the reactant to the peridotite of interest has simply increased the amount of liquid present in the experiment, and has not significantly affected the modal proportion of any other phase. Second, we have calculated the solid residue composition using the %*F* calculated by the RWB98 method (column 7, Table 6) and the analysed melt for each reaction experiment and performed mass balance calculations for the residue using the solid phases only. In every case except run TFB-12 (Table 6) we are able to demonstrate positive phase proportions and a very low residual sum (column 8, Table 6). This indicates that the compositions of the solid phases are appropriate for the residue of the peridotite of interest at the stated *P* and *T*. In the case of TFB-12, the composition of the added reactant was significantly different (as reflected in a residual sum for the residue of >1; see column 8, Table 6) from the expected equilibrium melt of the peridotite of interest so that it has resulted in an equilibrium phase assemblage for a completely different peridotite composition (see further discussion below). As with direct melting experiments the %*F* for TQ was calculating by multiplying the values in column 7, Table 6, by 0·6.

In general, it is recommended that the above three steps should be applied to all experimental peridotite melting and reaction experiments. In our experience, mass balance with positive phase proportions with a very low residual sum is the most rigorous test of equilibrium, good analytical data and appropriateness of the results of peridotite reaction experiments to petrogenetic modelling. The method of RWB98 should not be applied to experimental data that do not satisfy the above general criteria. This is because their technique will produce a result for %*F* regardless of the quality of mass balance and may also calculate positive %*F* for mass balance calculations that demonstrate negative melt phase proportions. In these cases, the RWB98 results are internally contradictory.

EXPERIMENTAL RESULTS

Crystallization experiments

In this study, we have chosen to perform reversal experiments on the highest temperature liquid compositions identified by KG92 as anomalous (T-2140, 1400°C; T-2113, 1375°C) from the FG87 dataset. In Fig. 2, we project these two compositions into the molecular normative basalt tetrahedron and compare them with calculated equilibrium melt compositions using the equations of KG92. The calculated melt compositions of KG92 compared with the experimental glass compositions have significantly higher normative olivine and lower normative diopside contents (Fig. 2). Also shown in Fig. 2 are the reanalysed glass compositions normalized to the international glass standard VG-2, and the original basalt compositions placed as the melt component in the sandwich experiments of FG87. In the case of T-2140, the basalt reactant was MORB glass DSDP3-18-7-1 and for T-2113 it was the calculated equilibrium melt at 1300°C for Tinaquillo Lherzolite from the study of Jaques & Green (1980).

Crystallization experiments on T-2113 and T-2140 are presented in Tables 2 and 3. In both cases the glass compositions are liquids at the stated *P* and *T* of the

*Table 6: Results of %*F *calculations on Tinaquillo Lherzolite (TQ-40) and MORB Pyrolite (MPY-87) at 1 GPa*

No.	Run no.	*T* (°C)	Bulk compositions			Peridotite of interest					
			1	2	3	4	5	6	7	8	9
			%*F* (Petmix)	Residual	%*F* (RWB)	%*F* (Petmix)	Residual	%*F* (RWB)[1]	%*F* (RWB)[2]	Residual[3]	%*F* TQ
Tinaquillo Lherzolite											
Direct melting experiments on TQ-40											
1	T-4301	1495	n.a.	n.a.	n.a.	59·8(3)	0·0747	n.a.	60·5(3)	n.a.	36·3
2	T-4014	1411	n.a.	n.a.	n.a.	45·0(9)	0·0963	n.a.	41·4(4)	n.a.	24·8
3	T-4304	1409	n.a.	n.a.	n.a.	40·5(8)	0·0532	n.a.	39·9(3)	n.a.	23·9
4	T-4081	1381	n.a.	n.a.	n.a.	35·5(6)	0·0456	n.a.	35·3(2)	n.a.	21·2
5	T-3976	1349	n.a.	n.a.	n.a.	30·5(6)	0·0126	n.a.	28(1)	n.a.	16·8
6	T-4126	1314	n.a.	n.a.	n.a.	24·9(3)	0·0023	n.a.	23·9(4)	n.a.	14·3
Reaction experiments using TQ-40											
7	T-3629	1370	48·3(4)	0·0130	48·4(3)	35(1)	0·1163	36·2(3)	34·8(5)	0·2761	20·9
8	TFB-11	1380	49(1)	0·1840	47·0(3)	35(1)	0·1071	34·8(3)	34·4(4)	0·3038	20·6
9	TFB-12	1371	49(1)	0·0917	48·9(3)	33(2)	0·4753	35·0(3)	33·7(4)	1·0944	20·2
10	T-4080	1344	67·1(5)	0·0302	67·2(3)	33(1)	0·1238	36·0(2)	32·3(4)	0·3543	19·4
11	T-4321	1359	46·7(2)	0·0046	46·8(3)	29·5(8)	0·0699	28·5(3)	29·4(3)	0·1421	17·6
12	T-4125	1325	52·9(4)	0·1840	52·5(4)	26(1)	0·0576	24·1(4)	23·2(6)	0·3151	13·9
13	T-3980	1310	31·6(6)	0·0195	29·5(4)	21·0(6)	0·0219	20·4(4)	19·9(4)	0·0661	11·9
14	T-3981	1321	35·0(3)	0·0032	34·8(3)	22(2)	0·1951	24·0(3)	20·8(6)	0·3380	12·5
MORB Pyrolite											
Direct melting experiments on MPY-87											
15	T-4306	1441	n.a.	n.a.	n.a.	37·3(2)	0·0313	n.a.	37·3(4)	n.a.	n.a.
16	T-4298	1371	n.a.	n.a.	n.a.	28·0(7)	0·0367	n.a.	28·1(4)	n.a.	n.a.
17	T-4297	1328	n.a.	n.a.	n.a.	23(2)	0·2968	n.a.	23·1(4)	n.a.	n.a.
Reaction experiments using MPY-87											
18	T-4183	1363	42(1)	0·1198	43·7(2)	28·9(6)	0·0351	28·6(2)	28·7(1)	0·0696	n.a.
19	T-4318	1355	36·4(9)	0·0897	37·7(2)	26(1)	0·0055	26·4(2)	26·5(2)	0·1199	n.a.
20	T-4284	1349	35(1)	0·1164	35·3(4)	25(1)	0·0613	24·8(4)	25·0(4)	0·1118	n.a.
21	T-4296	1336	50(1)	0·1709	50·0(2)	24(1)	0·1143	23·7(2)	24·5(2)	0·2009	n.a.
22	T-4338	1330	54(1)	0·0921	53(2)	25·1(8)	0·0674	24·0(1)	23(1)	0·2375	n.a.
23	T-4324	1325	32(1)	0·0165	31(1)	20·1(1)	0·0162	19(1)	20(1)	0·0259	n.a.

'RWB' refers to Robinson *et al.* (1998). Numbers in columns 3, 6 and 7 are the average weighted mean %*F* calculated using the method of Robinson *et al.* Numbers in parentheses in columns 3, 6 and 7 are the standard error on the %*F* calculation of those workers; e.g. 35·2(9) refers to 35·2 with a standard error of $\pm$0·9. '%*F* (Petmix)' refers to the %*F* calculated by least-squares linear regression using the software Petmix. Numbers in parentheses in columns 1 and 4 are 1σ in terms of the last units cited; e.g. 59·8(3) refers to 59·8$\pm$0·3. 'Residual' refers to the sum of the squares of the residuals for the Petmix calculation. '%*F* (RWB)[1]' refers to %*F* calculated using the solid modes present in the actual experiment of interest as determined by Petmix, and '%*F* (RWB)[2]' refers to the %*F* calculated using the solid modes present in the peridotite of interest as determined by Petmix (see text for details). 'Residual[3]' refers to the sum of the squares of the residuals for the Petmix calculations using the residual crystals in the experiment and the calculated residue composition for the peridotite of interest. The %*F* values in column 7 were used to calculate the residue composition. Column 9 lists the calculated %*F* (0·6 $\times$ %*F* in column 7) for Tinaquillo Lherzolite (TQ, Table 1, not the minus 40 wt % olivine composition TQ-40). In the case of direct melting experiments, bulk compositions and peridotite of interest are equivalent so results are presented only in columns 4–9. Temperature (°C) is the calculated OLT using the Ford *et al.* (1983) geothermometer (Tables 2 and 3).

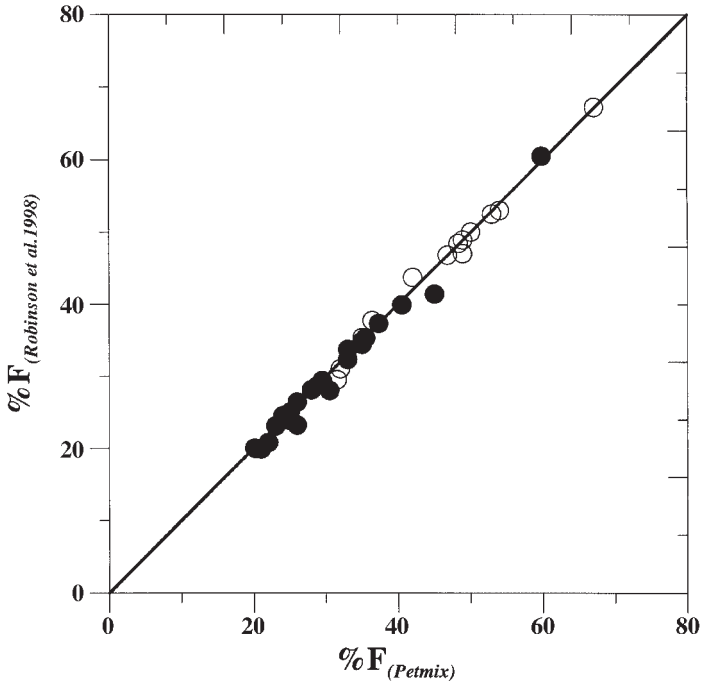

Fig. 1. %*F* calculated by least-squares linear regression (using software Petmix) vs the average weighted mean %*F* calculated using the method of Robinson *et al.* (1998). ●, results for the peridotite of interest (column 4 vs column 7, Table 6); ○, results for the bulk compositions of peridotite reaction experiments (column 1 vs column 3, Table 6).

original experiments (FG87) but their liquidus temperatures are significantly lower and the liquidus phase is clinopyroxene. The results of our crystallization experiments for T-2113 are identical to those obtained by KG91, demonstrating agreement between the techniques used in the various laboratories. To check for liquidus depression by inadvertent access of H_2O, we have measured H_2O in four of these runs by FTIR spectroscopy, finding <0·1% H_2O (Table 5).

We have investigated the possibility of incorrect temperature measurement by calculating the anhydrous olivine liquidus temperatures of the entire FG87, 88 dataset. The calculated liquidus temperatures are compared with experimental temperatures in Fig. 2. Falloon & Danyushevsky (2000) have demonstrated that the Ford *et al.* (1983) olivine geothermometer can reproduce the experimental olivine liquidus temperatures (OLT) of anhydrous olivine-saturated liquids to within experimental uncertainty of ± 15°C. As can be seen from Fig. 3 the reported experimental temperatures are either too high (FG87, series A; FG88, series A) or too low (FG87, series B), and this aspect is discussed further in a later section. We have investigated the question of compatibility of liquid and residual lherzolite mineralogy by performing additional reaction experiments and direct melting experiments on the MPY-87 and TQ-40 peridotite compositions. The results of these experiments are presented below.

The sandwich experiments performed by FG87 and FG88 can be divided into three series (A, B and C; see Appendix A). Both series A and B experiments used graphite inner capsules with a platinum outer capsule. However, the series A experiments used a larger graphite capsule than the series B experiments. The series C experiments (FG88 only) used graphite capsules only. The series A and C experiments used a $Pt_{90}/Pt_{90}Rh_{10}$ (Pt) thermocouple whereas the series B experiments used a $W_{97}Re_3/W_{75}Re_{25}$ (W/Re) thermocouple. The temperatures given by the tungsten/rhenium thermocouples were accepted as correct by Falloon & Green (1987, 1988) and the temperatures of the series A and C experiments were corrected (using an olivine *mg*-number vs *T* correlation) to the temperatures defined by the series B experiments, because of suspected drift of the Pt thermocouple in the reducing environment of the high-pressure piston-cylinder assembly (Holloway & Wood, 1988). In Appendix A, we report the original nominal uncorrected run temperatures, as well as the 'corrected' temperatures of FG87, FG88, and the newly calculated anhydrous and hydrous run temperatures based on the olivine thermometer of Ford *et al.* (1983). From Fig. 3 and Appendix A, it appears clear that both access of water (series A experiments) and use of W/Re vs Pt/Rh thermocouples have resulted in incorrect temperature determinations for experimental glasses in the FG87, FG88 data.

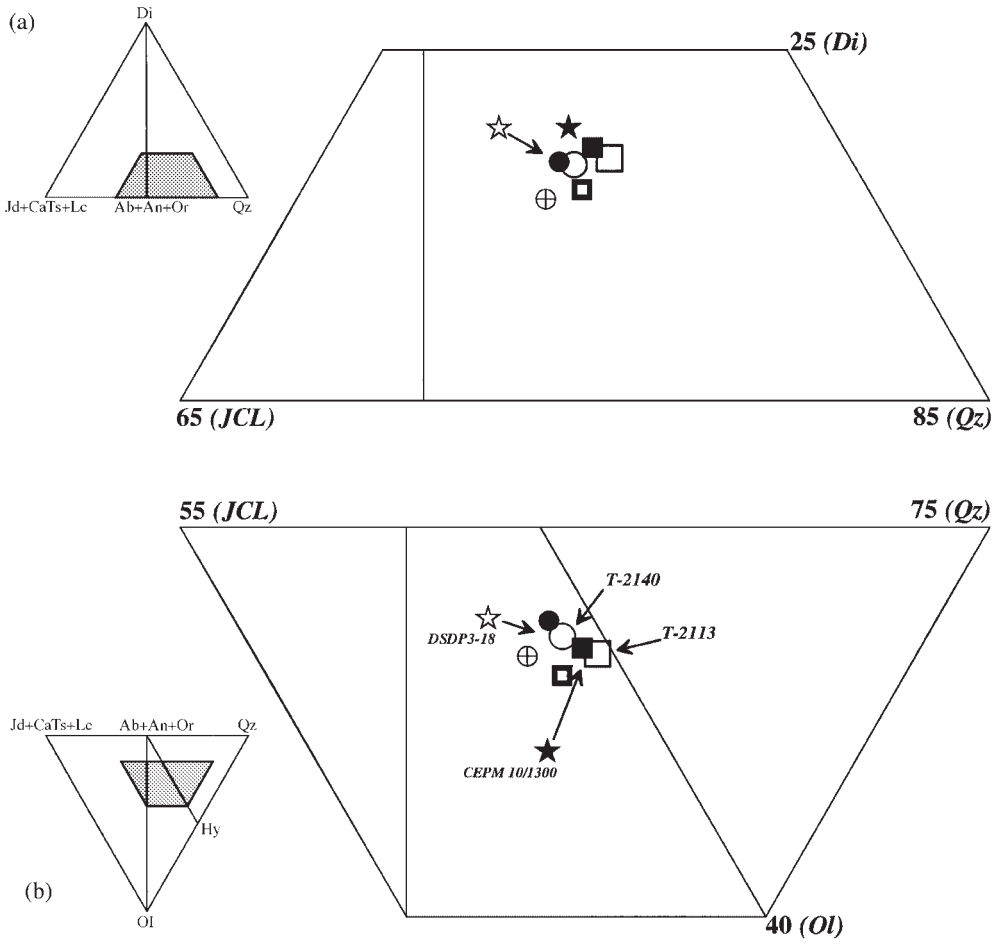

Fig. 2. Comparison of glass compositions from sandwich experiments (runs T-2140 and T-2113) from FG87 with calculated equilibrium melt compositions using the parameterization of KG92 for melt compositions in equilibrium with a spinel lherzolite residual assemblage, and the compositions of the initial reactants used in the sandwich experiments of FG87 in the molecular normative projection from Ol (a) onto the face (Jd + CaTs + Lc)–Di–Qz and from Di (b) onto the base (Jd + CaTs + Lc)–Qz–Ol of the 'basalt tetrahedron' (FG88, see insert). ○, glass composition from run T-2140 (FG87); ●, reanalysed glass compositions from run T-2140, this study (Appendix B); □, glass composition from run T-2113 (FG87); ■, reanalysed glass composition from run T-2113, this study (Appendix B); ☆, MORB glass reactant DSDP3-18-7-1 used in experiment T-2140; ★, reactant CEPM 10/1300 (Table 1) used in experiment T-2113; crossed circle, calculated equilibrium melt using the compositional parameters of the glass from T-2140 and the equations of Kinzler & Grove (1992); small □, calculated equilibrium melt using the compositional parameters of the glass from run T-2113 and the equations of Kinzler & Grove (1992).

As can be seen from Fig. 3, the plotted data can be broadly divided into three groups. Series A experiments of FG87 and FG88 have higher calculated OLT than the uncorrected experimental liquidus temperature—we infer that this was due to water access (Table 5). Series C and B experiments of FG88 have, in most cases, calculated OLT equal to the uncorrected liquidus temperature—we infer that the 'uncorrected' temperatures were correct within experimental error. Most series B experiments of FG87 have lower calculated OLT than their experimental temperature (Fig. 3, Appendix A). Of particular significance is that the T-2113 glass composition in experiments T-4320 and T-4300 has calculated anhydrous OLT (1327°C) that is identical to its experimentally determined liquidus within experimental uncertainties (±15°C). Also, both the original T-2113 glass and the crystallization experiments (T-4320, T-4300) on the T-2113 compositions have identical H_2O contents (~0·05–0·08 wt %, Table 5). These two observations support the hypothesis that the originally reported (1375°C) liquidus temperature of run T-2113 was anomalously high as a result of oxidation of the W/Re thermocouple. Oxidation of the W/Re thermocouple changes the e.m.f. of the thermocouple such that although the displayed run temperature of the experiment is controlled to within ±1°, the actual temperature in the experimental charge is lower, and falls with progressive oxidation. If oxidation is rapid, then an obvious power

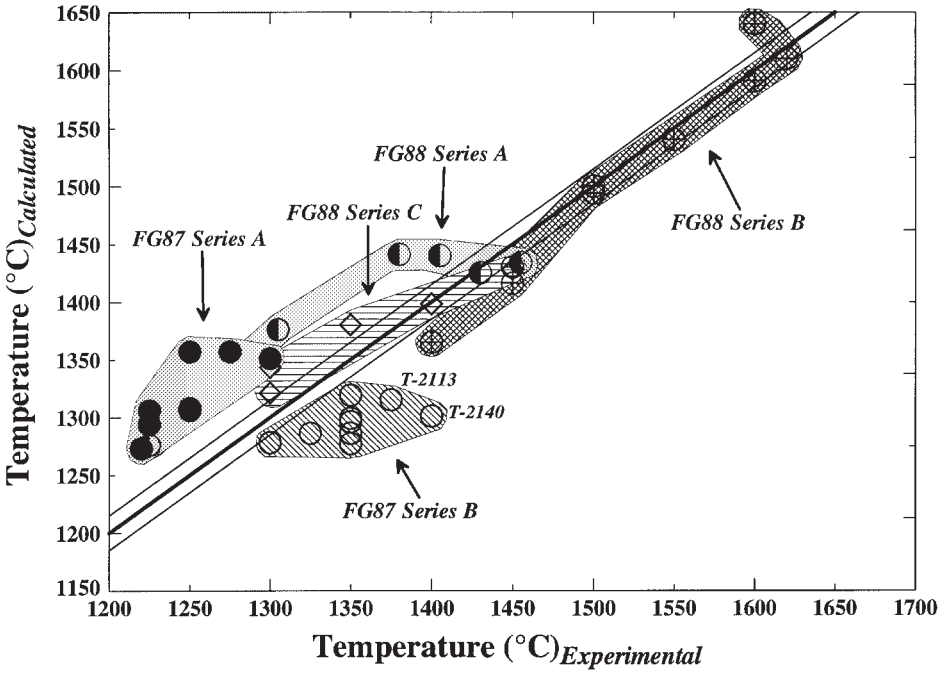

Fig. 3. Calculated olivine liquidus T (Appendix A) using the olivine geothermometer of Ford *et al.* (1983) vs the nominal run T (Appendix A) for the nominally anhydrous glasses from the sandwich experiments of FG87 and FG88. ●, series A experiments of FG87; ○, series B experiments of FG87; ◐, series A experiments of FG88; crossed circles, series B experiments of FG88; ◇, series C experiments of FG88. (See text for series definitions.)

decrease to the experimental assembly is observed. However, if oxidation is occurring slowly then it may not be possible to observe any significant power decrease.

In contrast to T-2113, the glass composition from T-2140 has a calculated OLT slightly lower (1319°C) than its experimentally determined liquidus (~1338°C, Table 3). From Fig. 3 we infer that the problematic behaviour of W/Re thermocouples at 1 GPa is not evident at >1 GPa (FG88, series B) and that series A experimental techniques permitted a depression of the liquidus of ~50–70°C as a result of access of water (Table 5).

Reaction and melting experiments

Two new series of reaction and melting experiments were performed using the MPY-87 and TQ-40 peridotite compositions. Series D reaction and melting experiments were performed to test whether despite the uncertain temperature of experiments T-2113 and T-2140, the glass compositions from runs T-2113 and T-2140 still represent equilibrium melts of TQ-40 and MPY-87, respectively, at temperatures to be determined. The series E reaction and melting experiments were performed over a temperature range at 1 GPa as part of our evaluation of the sandwich technique as a reliable method for determining equilibrium mantle melt compositions.

Series D reaction and melting experiments

The results of the series D reaction experiments (Table 3 and 4) are presented in Figs 4 and 5. We first performed reaction experiments at the stated temperature (i.e. 'corrected' T) of FG87 for both T-2113 and T-2140. In the case of T-2140, we used the synthetic mix of the T-2140 composition, and in the case of T-2113, we used the calculated equilibrium melt from Jaques & Green (1980) (CEPM 10/1300). In both cases (run T-3629, Table 2, Fig. 4; run T-4083, Table 3, Fig. 5) the residue was not spinel lherzolite but either harzburgite (T-3629) or dunite (T-4083). In addition, the resultant glass compositions after reaction are significantly different from both T-2113 and T-2140 (Figs 4 and 5). The results of these experiments indicate that both T-2113 and T-2140 are not equilibrium melts of TQ-40 or MPY-87 respectively at the stated P and T of FG87, consistent with the conclusions of KG91, KG92. We also performed reaction experiments at the *calculated* OLT of both T-2113 (1327°C) and T-2140 (1319°C) to test whether these glass compositions are in equilibrium with a spinel lherzolite residue (as observed in the experiments of FG87, but at lower temperatures).

In run T-3635 (at 1325°C, 1 GPa), we reacted the CEPM 10/1300 composition with TQ-40 and obtained a glass in equilibrium with spinel lherzolite. As the glass composition is identical to T-2113 (Table 2, Fig. 4), we

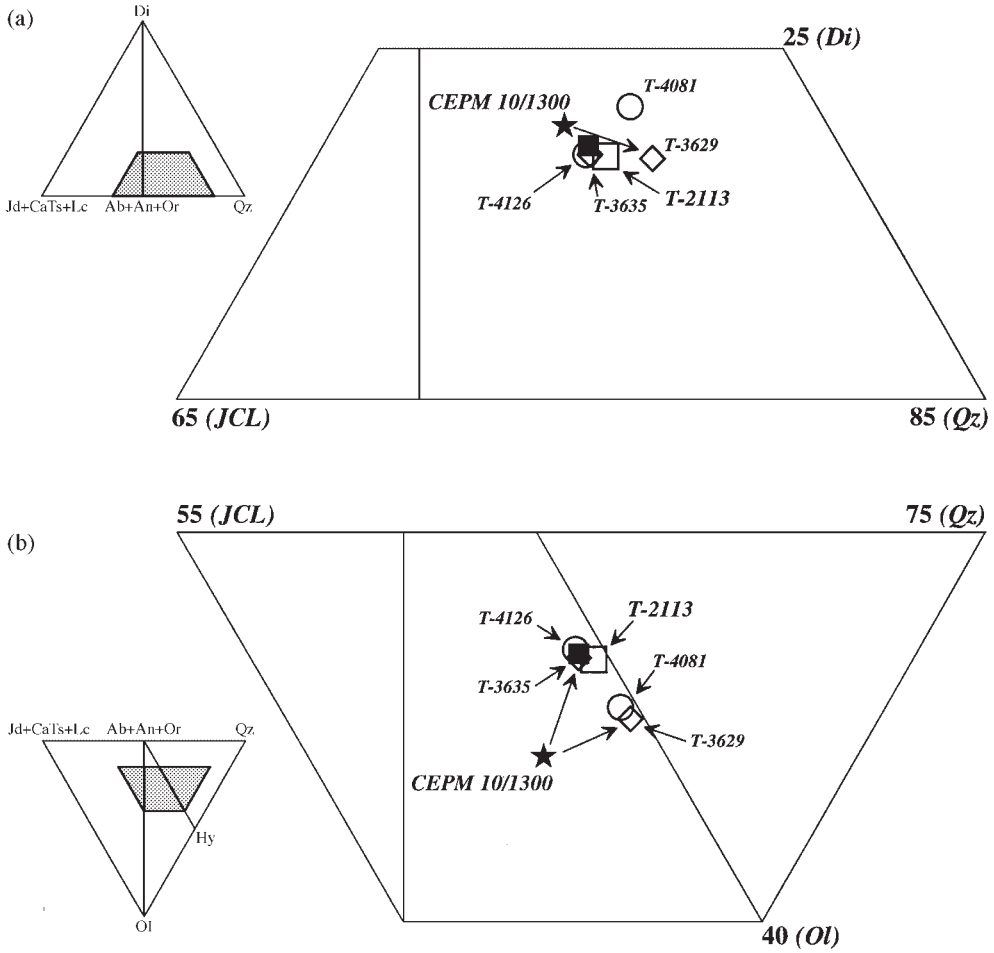

Fig. 4. Comparison of glass compositions from series A peridotite melting and reaction experiments on TQ-40 (Table 2) with the glass composition from run T-2113 in the molecular normative projection from Ol (a) onto the face (Jd + CaTs + Lc)–Di–Qz and from Di (b) onto the base (Jd + CaTs + Lc)–Qz–Ol of the 'basalt tetrahedron'. ○, glass compositions from direct melting experiments T-4126 and T-4081; ◇, glass compositions from reaction experiments T-3635 and T-3629; ★, initial reactant composition CEPM 10/1300 (Table 1) used in the series A reaction experiments; ■, reanalysed glass composition from run T-2113, this study (Appendix B); □, glass composition from run T-2113 (FG87).

infer that T-2113 is indeed an equilibrium melt of TQ-40 at a corrected temperature of ~1325°C. To further test this conclusion, we performed two reversal experiments using the TQ-40 composition, without the basalt layer. In run T-4126, we held the TQ-40 composition at 1500°C for 1 h before bringing the run temperature to 1325°C. A high-temperature olivine + liquid phase assemblage recrystallized to a lower-temperature spinel lherzolite + liquid assemblage, over a 24 h period. As can be seen from Fig. 4, the glass in run T-4126 is almost identical to the glass composition from run T-2113 and T-3635. In a similar manner, run T-4081 was initially held at 1500°C for 1 h before temperature was lowered to 1375°C. Run T-4081 resulted in a harzburgite residue and a glass (Fig. 4) that is very similar to the glass in run T-3629. In summary, our crystallization, reaction and direct melting reversal experiments demonstrate that run T-2113 is an equilibrium melt of TQ-40 at 1325°C leaving a lherzolite residue and that the equilibrium assemblage of TQ-40 at 1375°C is harzburgite + liquid (see Table 4).

For the MP-87 composition, in run T-4296 we reacted the T-2140 composition at its experimentally determined liquidus of 1338°C and in run T-4324 we reacted the T-2140 composition at its calculated OLT (1320°C) (Table 3). Run T-4296 resulted in a harzburgite residue and run T-4324 resulted in a spinel lherzolite residue. As can be seen from Fig. 5b, the glass compositions from both T-4296 and T-4324 are significantly different from the glass in run T-2140, suggesting that run T-2140 did not achieve equilibrium during thermocouple and temperature drift in the original experiment. In summary,

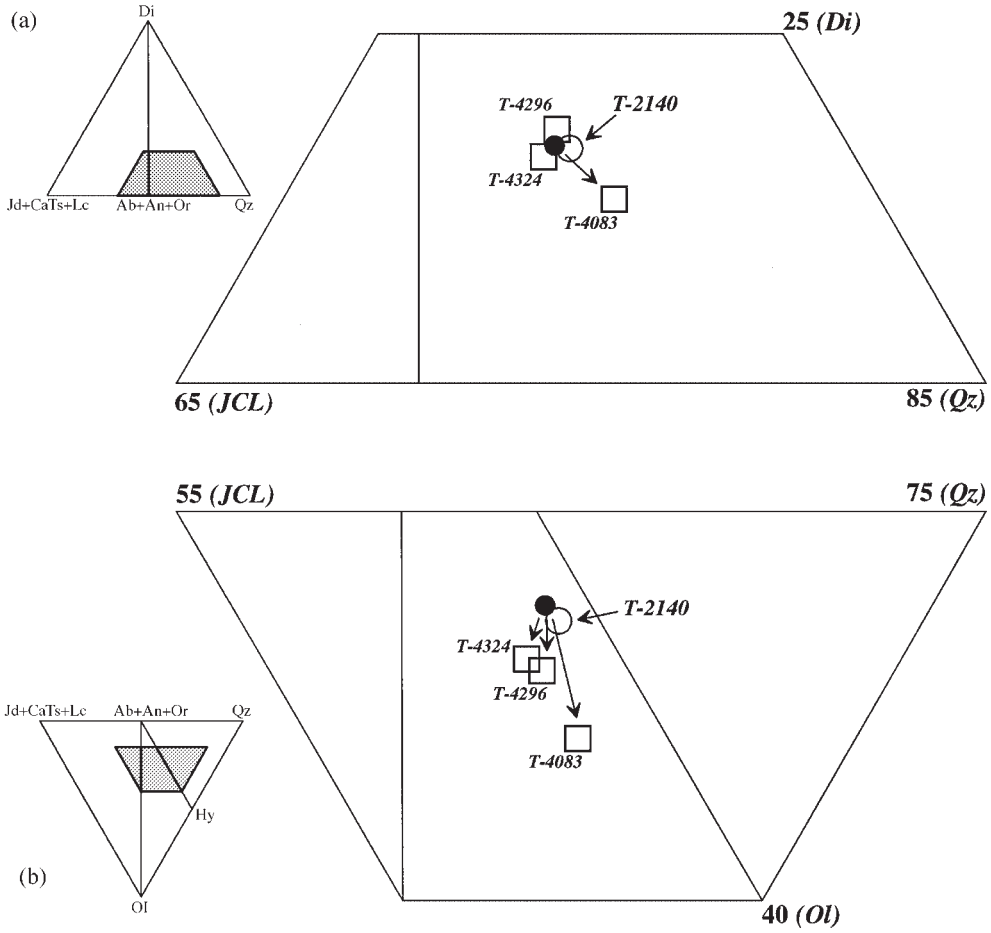

Fig. 5. Comparison of glass compositions from series A peridotite reaction experiments on MPY-87 (Table 3) with the glass composition from run T-2140 in the molecular normative projection from Ol (a) onto the face (Jd + CaTs + Lc)–Di–Qz and from Di (b) onto the base (Jd + CaTs + Lc)–Qz–Ol of the 'basalt tetrahedron'. □, glass compositions from reaction experiments T-4324, T-4296 and T-4083; ●, reanalysed glass composition from run T-2140, this study (Appendix B); ○, glass composition from run T-2140 (FG87).

our reversal experiments on the T-2140 composition of FG87 demonstrate that it is not an equilibrium melt of MPY-87 composition, as there is a consistent shift in composition when it is reacted at its stated T (1400°C), its experimentally determined liquidus (1338°C) and at its calculated OLT (1320°C).

The contrasting results from our reversal experiments on the T-2113 (equilibrium) and T-2140 (non-equilibrium) glass compositions provide insight into the FG87 dataset that used the W/Re thermocouple. All the runs (nine experiments, see Appendix A) of that study, except one (T-2078, which was initially overpressed to 2 GPa), performed using the W/Re thermocouple have suffered varying degrees of temperature drift to lower values (as a result of oxidation?) during the course of the experiments (average 1·8 ± 0·8°C/h). Thus 'true' run temperatures are significantly lower than published by FG87 (see Appendix A). Because those workers used fine-grained synthetic starting materials, equilibrium between crystals and melts was, in most cases, maintained during this progressive temperature drop, resulting in fully equilibrated and homogeneous run products, as demonstrated by the reversal experiments on the T-2113 composition at 1325°C. On the basis of our results, the most important factor determining whether a bulk composition maintains equilibrium despite progressive temperature fall as a result of oxidation of the W/Re thermocouple is not the absolute temperature fall, but the rate of fall. In our experience, runs with >2·6°C/h temperature drop owing to oxidation of the W/Re thermocouple should be treated with caution. In the case of the FG87 series B experiments, both runs T-2140 and T-2123 suffered rates of decrease >3·5°C/h. In these two experiments, the glass has failed to maintain equilibrium with olivine as temperature has declined, as demonstrated by reversal experiments on the T-2140 glass composition.

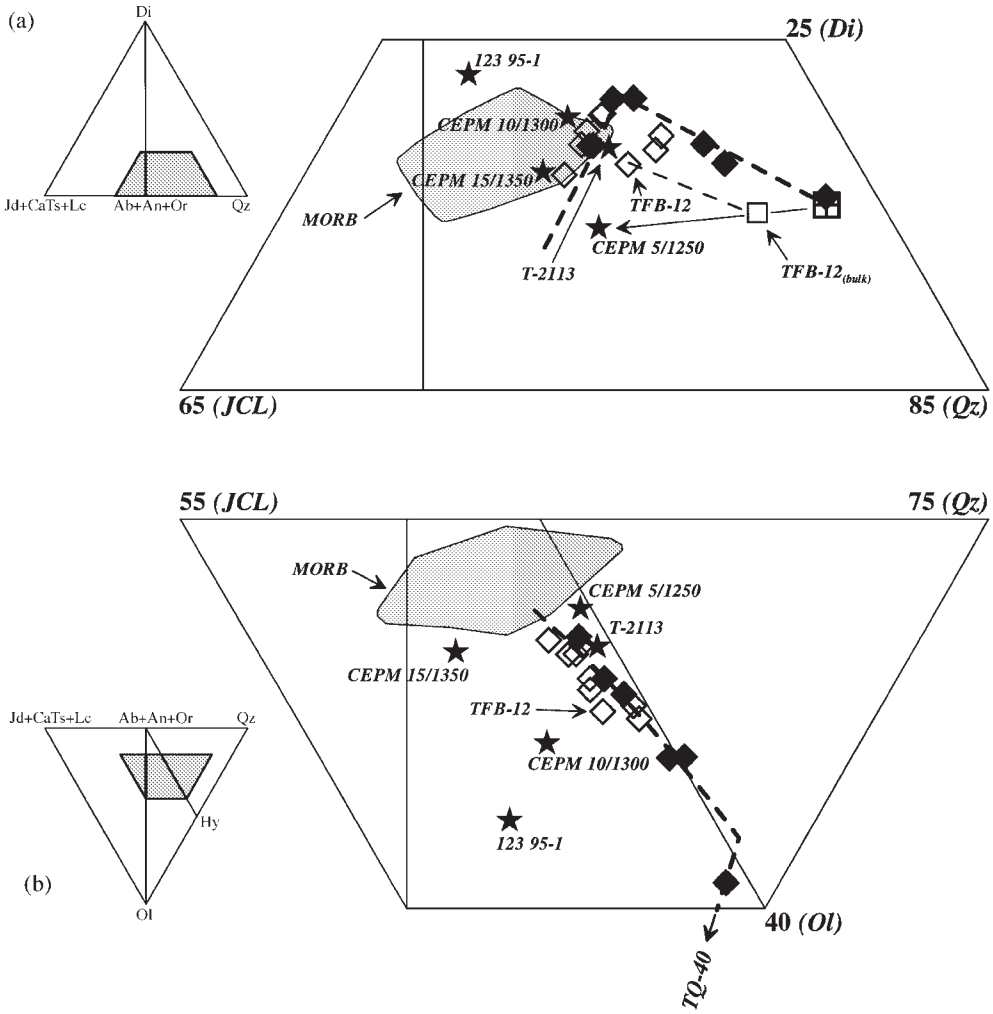

Fig. 6. Comparison of glass compositions from series B peridotite melting and reaction experiments on TQ-40 (Table 2) in the molecular normative projection from Ol (a) onto the face (Jd + CaTs + Lc)–Di–Qz and from Di (b) onto the base (Jd + CaTs + Lc)–Qz–Ol of the 'basalt tetrahedron'. ◆, glass compositions from direct melting experiments on TQ-40; ◇, glass compositions from peridotite reaction experiments on TQ-40; ★, compositions of initial reactants in the peridotite reaction experiments (Table 1); crossed square in (a), composition of TQ-40; dashed line, equilibrium mantle melting cotectic for TQ-40 at 1 GPa based on the results of this study and T. J. Falloon (unpublished data, 1999); filled field labelled MORB encloses the compositions of 50 primitive glasses *mg*-numbers ≥ 0·68 (for data sources see caption to fig. 4 of FG87).

Series E reaction and melting experiments

To evaluate the sandwich technique as a suitable method for determining mantle melt compositions at 1 GPa independent of the thermocouple drift problems, additional peridotite reaction experiments were performed on the MPY-87 and TQ-40 compositions to compare with the results of direct melting experiments (Tables 3 and 4). In the case of TQ-40, basalt compositions of significantly different normative compositions (10/1300, 5/1250, 15/1350 and T-2113, Table 1) were used. In the case of MPY-87, the T-2140 composition was used (Table 3). The rationale of the series E reaction experiments was to demonstrate that using different basaltic layer compositions (but all derived from TQ-40 at a different *P*, *T* condition), the resulting glass compositions defined the same mantle melting cotectic as defined by direct melting experiments on the respective peridotite compositions (Tables 3 and 4). The results of the series E experiments are presented in Figs 6–9. In view of the potential uncertainties caused by the possible presence of H_2O in nominally anhydrous experimental glasses and thermocouple drift during experiments, we have used the calculated anhydrous olivine liquidus temperatures (using Ford *et al.*, 1983) for comparative purposes in Figs 8 and 9. As can be seen from Figs 6 and 7, the glass compositions from the reaction experiments (with the

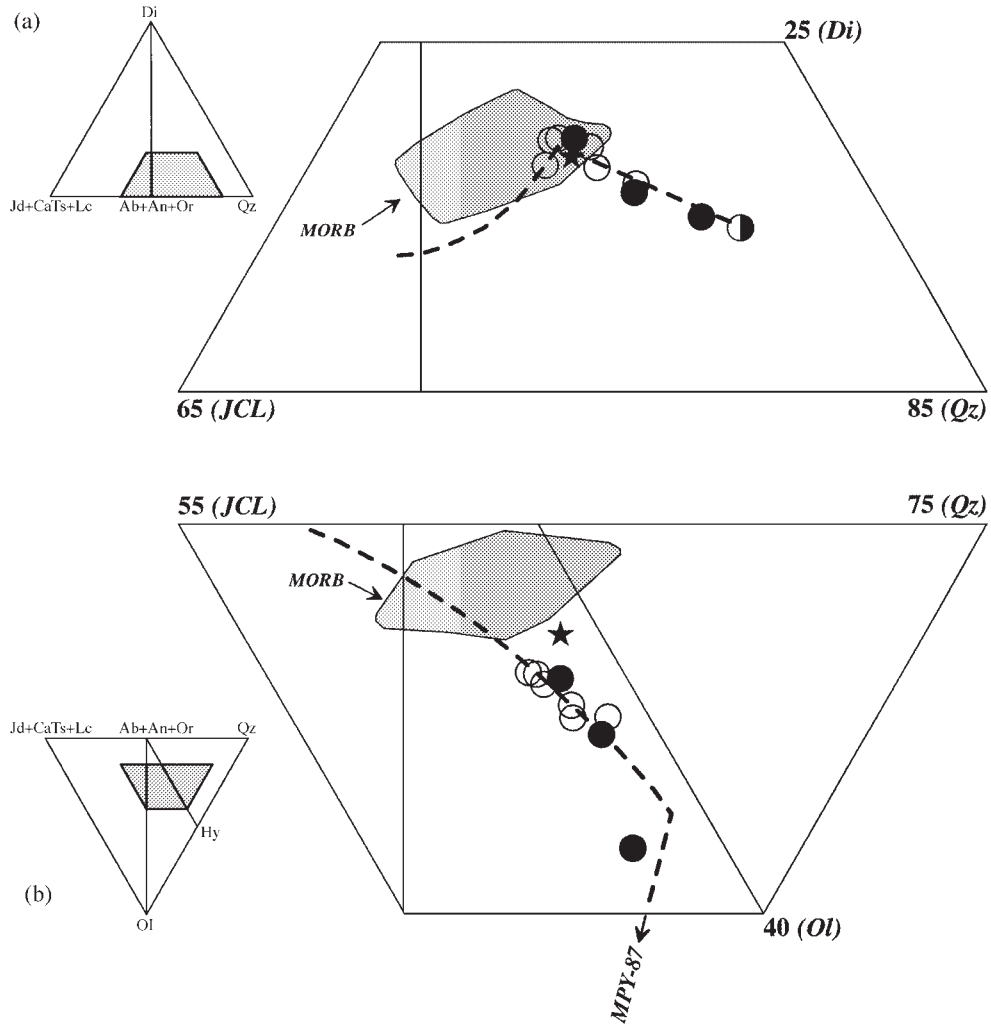

Fig. 7. Comparison of glass compositions from series B peridotite melting and reaction experiments on MPY-87 (Table 3) in the molecular normative projection from Ol (a) onto the face (Jd + CaTs + Lc)–Di–Qz and from Di (b) onto the base (Jd + CaTs + Lc)–Qz–Ol of the 'basalt tetrahedron'. ●, glass compositions from direct melting experiments on MPY-87; ○, glass compositions from peridotite reaction experiments on MPY-87; ★, compositions of initial reactant T-2140 in the peridotite reaction experiments (Table 1); half-filled circle in (a), composition of MPY-87; dashed line, equilibrium mantle melting cotectic for MPY-87 at 1 GPa based on the results of this study and T. J. Falloon (unpublished data, 1999); filled field labelled MORB encloses the compositions of 50 primitive glasses *mg*-numbers $\geqslant 0{\cdot}68$ (for data sources see caption to fig. 4 of FG87).

exception of TFB-12) define the same cotectics as the glass compositions from direct melting experiments on the respective peridotite compositions. Attention is drawn to the effects of changes in bulk composition (by mixing TQ-40 with different liquids) which shift the harzburgite residue trends in the projection from olivine. As can be seen from Fig. 8, the major element compositions of the reaction and direct melting glasses define the same trends with respect to temperature. Also, the direct melting and reaction experiments define the same %*F* trend [calculated with respect to lherzolite compositions MORB Pyrolite (*mg*-number 87) and Tinaquillo Lherzolite] with respect to temperature for the two peridotite compositions (Fig. 9), indicating that there are no significant differences in the residue compositions between reaction and direct melting experiments. Run TFB-12, although not anomalous in the projection from Di (Fig. 6b), has significantly lower normative Di in the projection from Ol (Fig. 6a). This simply reflects the fact that if the initial reactant is not chosen carefully, the resultant bulk composition may be unable to 'buffer' the differences between the reactant and actual equilibrium melt

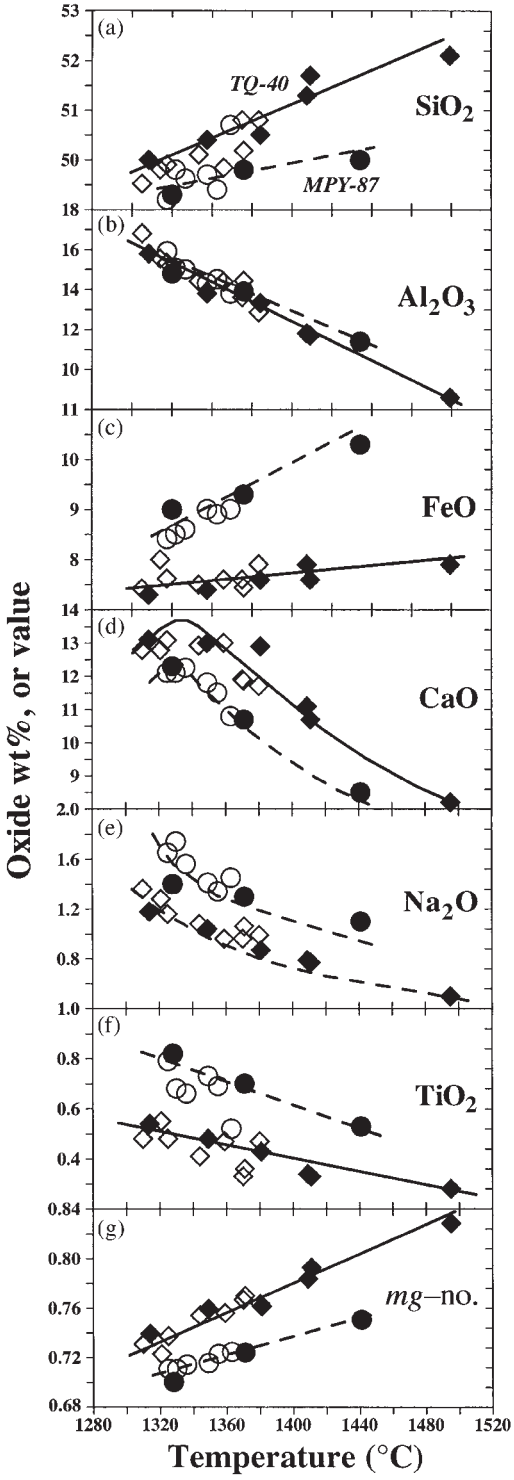

Fig. 8. A comparison of the wt % SiO_2 (a), Al_2O_3 (b), FeO (c), CaO (d), Na_2O (e), TiO_2 (f) contents and *mg*-number values (g) vs temperature (°C) between glass compositions from direct peridotite and peridotite reaction experiments on TQ-40 and MPY-87. Symbols as for Figs 5 and 6. Temperature is the calculated OLT using the Ford *et al.* (1983) geothermometer (Tables 2 and 3). *mg*-number = $Mg/(Mg + Fe^{2+})$, with total Fe calculated as Fe^{2+}.

composition for the model peridotite. In the case of TFB-12, the reactant was a low normative Di glass composition (CEPM 5/1250, Table 1) and the liquid in equilibrium with harzburgite residue reflects the low normative diopside content of the bulk composition.

DISCUSSION

Our aim in this study was to re-evaluate several 'anomalous' results identified by others in our earlier studies (FG87, 88), and to understand the technical reasons for these results. By these and additional experiments, we provide here datasets for melt and residual mineral compositions at 1 GPa on two lherzolite compositions, MP-87 and TQ-40, which define progressive melting from ~1300°C to 1450°C. The availability of such quantitative data is a necessary step in both formulating and evaluating generalized models of peridotite melting that can be applied to different mantle compositions. In carrying out this study, we confirm that uncertainties and errors can be introduced into experimental studies by difficulty in controlling access of water and by behaviour of thermocouples, particularly in drift to lower temperature during oxidation of the W/Re thermocouple at low pressure (<1·5 GPa).

H_2O contents of 'anhydrous' experiments

Falloon & Danyushevsky (2000) have demonstrated that the Ford *et al.* (1983) olivine geothermometer can be used to calculate the olivine liquidus temperatures for anhydrous compositions to within ±15°, and as can be seen from Fig. 3 a number of experiments (FG88, series B and C) have experimental and calculated liquidus temperatures consistent with the Ford *et al.* (1983) relationship. However, it is also evident from Fig. 3 and Tables 2 and 3 that a number of experimentally determined liquids have calculated OLT >15°C (including runs T-1511, T-1478, T-1480, T-4301, TFB-11, TFB-12 and T-4318) above their nominal run temperatures. This effect could be explained by small amounts of H_2O in the experimental glasses. We have tested this by analysing these glasses for H_2O by FTIR spectroscopy, and these results are presented in Table 5 and Fig. 10. The analysed H_2O contents of these glasses are consistent with the expected olivine liquidus depression based on the study by Falloon & Danyushevsky (2000), as can be seen from Fig. 10. We also analysed for H_2O some glasses that had calculated OLT within 15°C of their nominal temperatures (runs T-3629, T-3980, T-3981, T-4284). The H_2O contents of these glasses varied from 0·04 to 0·15 wt %. On the basis of the empirical relationship of Falloon & Danyushevsky (2000), these H_2O contents should have resulted in a liquidus depression of between

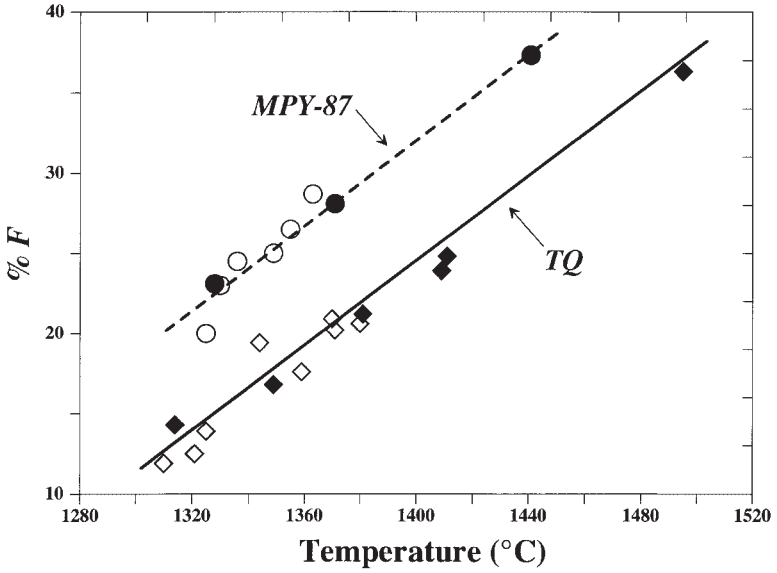

Fig. 9. The variation of the calculated %*F* (wt %) with temperature (°C) for the peridotite compositions MPY-87 and Tinaquillo Lherzolite (TQ, not the minus 40% olivine composition TQ-40). Symbols as for Figs 6 and 7. %*F* is calculated by the method of Robinson *et al.* (1998) (column 7, Table 6, for MPY-87; column 9, Table 6, for TQ). Temperature is the calculated OLT using the Ford *et al.* (1983) geothermometer (Tables 2, 3 and 6).

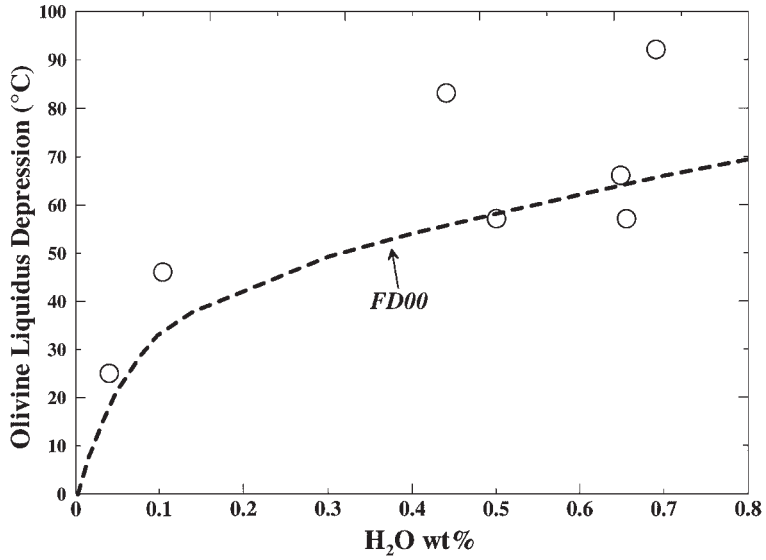

Fig. 10. The calculated liquidus depression for runs T-1511, T-1478, T-1480, T-4301, TFB-11, TFB-12 and T-4318 vs analysed H_2O in wt % (Table 5). Dashed line, empirical expression for the olivine liquidus depression from Falloon & Danyushesvky (2000).

24 and 38°C. Possible explanations for the absence of observable depressions are as follows: (1) as these experiments all used the W/Re thermocouple, it is possible that the W/Re thermocouple suffered minor amounts of oxidation (between–0·6 and 2°C/h); (2) there is a 'background level' of ~0·05% H_2O contents in nominally anhydrous experiments, present even in the experiments of the dataset used by Ford *et al.* (1983) to calibrate their olivine geothermometer. At present, we do not have sufficient data to distinguish between these

possibilities, and further FTIR analyses of H_2O contents of nominally anhydrous experimental glasses are required (work in progress).

Evaluation of the sandwich technique

Our experimental study, utilizing fine-grained synthetic starting materials, demonstrates that the sandwich technique is an effective approach for determining the compositions of mantle melts and important petrogenetic parameters such as the variation of $\%F$ with temperature. Our experimental study also demonstrates the utility of the olivine geothermometer of Ford *et al.* (1983), combined with FTIR analysis of H_2O in experimental glasses, in evaluating thermocouple performance during mantle melting experiments. Some of the criticisms of the sandwich technique are based on misconceptions of the concept of 'multiple saturation' or on disagreements among peridotite melting studies using natural mineral mixes as starting materials. For example, Hirose & Kushiro (1993), using the diamond aggregate technique, criticized the sandwich technique because their experimental results differed from those of Takahashi & Kushiro (1983) for the same peridotite composition HK-66. Both studies used natural mineral mix starting materials, and, as demonstrated by Falloon *et al.* (1999*a*), such studies are likely to produce erroneous results no matter what technique is used (i.e. direct melting, diamond-aggregate entrapment, sandwich).

The recommended approach is to perform direct melting experiments first on a fine-grained, sintered mix of the composition of the peridotite of interest, establishing the composition of residual phases and an estimate (including mass balance) of the liquid composition and phase projections. This estimated melt composition can then be used as a reactant in sandwich experiments, with the expectation that a large pool of liquid, free of quench modification, will be present, along with residual phases matching those of the forward experimental work with intergranular (quench-modified) melt of the same composition as in the layer.

Melt compositions at 1 GPa

Projection of bulk compositions and melt compositions into the 'basalt normative tetrahedron' illustrates that the lower temperature melting trend is constrained to lie on an olivine + orthopyroxene + clinopyroxene ($\pm$ Cr spinel) cotectic and the shift of liquid compositions onto olivine + orthopyroxene cotectics occurs (as expected) at higher temperatures. The effect of varying bulk composition (by addition of the basaltic sandwich layer) in controlling the harzburgite trend is well illustrated in the projection from olivine (Fig. 6a, especially run TFB-12). In the plots of oxides vs temperature [Ford *et al.* (1983) temperature at 1 GPa], only CaO (Fig. 8d) shows change in slope as the residue changes from lherzolite to harzburgite. The differences in slopes of the SiO_2, FeO vs temperature plots of the MPY-87 and TQ-40 compositions reflect the different *mg*-number and FeO contents of the two compositions. The difference in refractoriness between the two compositions is also apparent in Fig. 9, where, at 1320°C, the melt fraction present in the Tinaquillo Lherzolite composition is 11–14%, whereas it is 20–23% in the MORB Pyrolite composition. However, within the 10–40% melting range, the rate of increase of melt fraction with rise in temperature is very similar for the two compositions and largely represents solution of olivine + orthopyroxene + minor spinel.

ACKNOWLEDGEMENTS

We would especially like to thank Ro Kinzler and Tim Grove for discussions on this work, for allowing us to see their unpublished reversal work on the Falloon & Green (1987) glass composition T-2113, and for kindly providing the starting material of the T-2113 glass used in their study. Both T.J.F. and L.V.D. acknowledge support of the Australian Research Council, which provided research funds for this project. We acknowledge the technical assistance of Keith Harris, Stephen Lane, David Steele, Nick Ware and Graeme Rowbottom. We acknowledge support of the Museum of Natural History, Washington, DC, which provided electron microprobe standards. We also thank Bernie Wood and Richard Arculus for their constructive reviews of this paper.

REFERENCES

Baker, M. B. & Stolper, E. M. (1994). Determining the compositions of high-pressure melts using diamond aggregates. *Geochimica et Cosmochimica Acta* **58**, 2811–2827.

Danyushevsky, L. V., Falloon, T. J., Sobolev, A. V., Crawford, A. J., Carroll, M. & Price, R. C. (1993). The H_2O content of basalt glasses from Southwest Pacific back-arc basins. *Earth and Planetary Science Letters* **117**, 347–362.

Falloon, T. J. & Danyushevsky, L. V. (2000). Melting of refractory mantle at 1·5, 2 and 2·5 GPa under anhydrous and H_2O-undersaturated conditions: implications for the petrogenesis of high-Ca boninites and the influence of subduction components on mantle melting. *Journal of Petrology* **41**, 257–283.

Falloon, T. J. & Green, D. H. (1987). Anhydrous partial melting of MORB pyrolite and other peridotite compositions at 10 kbar and implications for the origin of primitive MORB glasses. *Mineralogy and Petrology* **37**, 181–219.

Falloon, T. J. & Green, D. H. (1988). Anhydrous partial melting of peridotite from 8 to 35 kbars and the petrogenesis of MORB. *Journal of Petrology Special Issue* 379–414.

Falloon, T. J., Green, D. H., O'Neill, H. St. C. & Hibberson, W. O. (1997). Experimental tests of low degree peridotite partial melt compositions: implications for the nature of anhydrous near-solidus peridotite melts at 1 GPa. *Earth and Planetary Science Letters* **152**, 149–162.

Falloon, T. J., Green, D. H., Danyushevsky, L. V. & Faul, U. H. (1999*a*). Peridotite melting at 1·0 GPa and 1·5 GPa: an experimental evaluation of techniques using diamond aggregates and natural mineral mixes for determination of near-solidus melts. *Journal of Petrology* **40**, 1343–1375.

Falloon, T. J., Green, D. H., Jaques, A. L. & Hawkins, J. W. (1999*b*). Refractory magmas in back-arc basin settings—experimental constraints on the petrogenesis of a Lau Basin example. *Journal of Petrology* **40**, 255–277.

Ford, C. E., Russell, D. G., Craven, J. A. & Fisk, M. R. (1983). Olivine–liquid equilibria: temperature, pressure and composition dependence of the crystal/liquid cation partition coefficients for Mg, Fe^{2+}, Ca and Mn. *Journal of Petrology* **24**, 256–265.

Fujii, T. & Scarfe, C. M. (1985). Compositions of liquids coexisting with spinel lherzolite at 10 kbar and the genesis of MORBs. *Earth and Planetary Science Letters* **90**, 18–28.

Green, D. H. & Falloon, T. J. (1998). Pyrolite: a Ringwood concept and its current expression. In: Jackson, I. (ed.) *The Earth's Mantle: Composition, Structure, and Evolution*. Cambridge: Cambridge University Press, pp. 311–378.

Green, D. H., Hibberson, W. O. & Jaques, A. L. (1979). Petrogenesis of mid-ocean ridge basalts. In: McElhinny, M. W. (ed.) *The Earth: its Origin, Structure and Evolution*. London: Academic Press, pp. 265–290.

Hirose, K. & Kushiro, I. (1993). Partial melting of dry peridotites at high pressures: determination of compositions of melts segregated from peridotites using aggregates of diamonds. *Earth and Planetary Science Letters* **114**, 477–489.

Holloway, J. R. & Wood, B. J. (1988). *Simulating the Earth: Experimental Geochemistry*. London: Unwin & Hyman.

Jaques, A. L. & Green, D. H. (1980). Anhydrous melting of peridotite at 0–15 kb pressure and the genesis of tholeiitic basalts. *Contributions to Mineralogy and Petrology* **73**, 287–310.

Jarosewich, E. J., Nelen, J. A. & Norberg, J. A. (1980). Reference samples for electron microprobe analyses. *Geostandards Newsletter* **4**, 257–258.

Johannes, W., Bell, P. M., Boettcher, A. L., Chipman, D. W., Hays, J. F., Mao, H. K., Newton, R. C. & Seifert, F. (1971). An interlaboratory comparison of piston-cylinder pressure calibration using the albite-breakdown reaction. *Contributions to Mineralogy and Petrology* **32**, 24–38.

Kelemen, P. B., Dick, H. J. B. & Quick, J. E. (1992). Formation of harzburgite by pervasive melt/rock reaction in the upper mantle. *Nature* **358**, 635–641.

Kinzler, R. J. & Grove, T. L. (1991). An experimental evaluation of liquids produced in peridotite–basalt sandwich experiments. *EOS Transactions, American Geophysical Union* **72**(44), 548.

Kinzler, R. J. & Grove, T. L. (1992). Primary magmas of mid-ocean ridge basalts 1. Experiments and methods. *Journal of Geophysical Research* **97**, 6907–6926.

Kushiro, I. (1996). Partial melting of a fertile mantle peridotite at high pressures: an experimental study using aggregates of diamond. In: Basu, A. & Hart, S. R. (eds) *Earth Processes: Reading the Isotopic Code*. Washington, DC: American Geophysical Union, pp. 109–122.

Robinson, J. A. C., Wood, B. J. & Blundy, J. D. (1998). The beginning of melting of fertile and depleted peridotite at 1·5 GPa. *Earth and Planetary Science Letters* **155**, 97–111.

Stolper, E. (1980). A phase diagram for mid-ocean ridge basalts: preliminary results and implications for petrogenesis. *Contributions to Mineralogy and Petrology* **74**, 13–27.

Takahashi, E. & Kushiro, I. (1983). Melting of a dry peridotite at high pressures and basalt magma genesis. *American Mineralogist* **68**, 859–879.

Walter, M. J. & Presnall, D. C. (1994). Melting behaviour of simplified lherzolite in the system $CaO–MgO–Al_2O_3–SiO_2–Na_2O$ from 7 to 35 kbar. *Journal of Petrology* **35**, 329–359.

APPENDIX A

Run temperatures from Falloon & Green (1987, 1988)

	P (GPa)	Nominal run *T* (°C)	'Corrected' *T* (°C)	Calculated anhydrous run *T* (°C)	H_2O (wt %)	Calculated hydrous run *T* (°C)
Series A (Pt/Rh thermocouple)						
Falloon & Green (1987)						
T-1511	1·0	1220	1310	1273	0·5	1215
T-1472	1·0	1250	1350	1308		
T-1493	1·0	1225	1350	1294		
T-1478	1·0	1225	1400	1306	0·44	1250
T-1464	1·0	1300	1420	1351		
T-1480	1·0	1275	1420	1357	0·69	1292
T-1461	1·0	1250	1420	1357		
Falloon & Green (1988)						
T-1516	0·8	1225	1350	1276		
T-1512	0·8	1250	1400	1306	0·4	1252
T-1479	1·2	1305	1450	1376	0·33	1326
T-1515	2·0	1455	1420	1434		
T-1501	2·0	1380	1430	1441		
T-1513	2·0	1405	1450	1440	0·63	1377
T-1499	2·0	1430	1475	1425		
Series B (W/Re thermocouple)						
Falloon & Green (1987)						
T-2123	1·0	1350	1350	1286		
T-2140	1·0	1400	1400	1301		
T-2113	1·0	1375	1375	1315	0·08	1284
T-2117	1·0	1325	1325	1286		
T-2133	1·0	1350	1350	1296		
T-2121	1·0	1350	1230	1277		
T-2078	1·0	1300	1300	1278		
T-2138	1·0	1350	1350	1299	0·08	1268
T-2136	1·0	1350	1350	1319		
Falloon & Green (1988)						
T-2189	1·2	1400	1400	1365		
T-2192	1·5	1450	1450	1416		
T-2056	1·5	1450	1450	1430		
T-2069	2·0	1500	1500	1494		
T-2207	2·0	1500	1500	1500		
T-2086	2·5	1550	1550	1540		
T-2065	3·0	1600	1600	1591		
T-2075	3·0	1620	1620	1610		
T-2087	3·5	1600	1600	1640		
Series C (Pt/Rh thermocouple)						
Falloon & Green (1988)						
T-1994	1·2	1300	1375	1321	0·04	1297
T-1989	1·5	1300	1360	1343		
T-1999	1·5	1350	1420	1380		
T-2029	1·8	1400	1370	1398		
T-2031	1·8	1450	1450	1428		

Anhydrous temperature (°C) is the OLT calculated using the olivine geothermometer of Ford *et al.* (1983). OLT values are calculated using the reanalysed glass compositions in Appendix B if available, otherwise the original glass composition as reported in FG87 and FG88 is used. 'Corrected' temperatures are those reported originally in FG87 and FG 88. Pt/Rh refers to the $Pt/Pt_{90}Rh_{10}$ thermocouple. W/Re refers to the $W_{75}Re_{25}/W_{97}Re_3$ thermocouple. Hydrous temperature (°C) is calculated using the empirical expression of Falloon & Danyushevsky (2000). H_2O wt % determined by FTIR spectroscopy.

APPENDIX B

Compositions of experimental run products from Falloon & Green (1987, 1988)

Run no.	Phase	MB	SiO_2	TiO_2	Al_2O_3	FeO	MnO	MgO	CaO	Na_2O	K_2O	Cr_2O_3
Falloon & Green (1987)												
T-1511	Olivine	0·56	40·41			12·15		47·54				
	Orthopyroxene	0·19	53·01	0·28	6·47	7·47	0·10	29·43	2·46	0·10		0·69
	Clinopyroxene	0·12	50·88	0·60	6·86	4·45	0·05	17·78	18·02	0·47		0·88
	Spinel	0·01	0·18	0·23	57·68	10·12	0·09	20·53	0·06			11·11
	Glass*	0·12	50·58	0·84	19·07	7·10		8·35	10·42	3·42		0·11
	Residual	0·0047										
T-1472	Olivine	0·54	40·74		0·22	11·22		47·60				0·24
	Orthopyroxene	0·16	53·53		5·61	6·80		30·33	2·82			0·91
	Clinopyroxene	0·07	50·82	0·35	7·27	5·03	0·15	19·03	16·08	0·46		0·81
	Spinel	0·01	0·35	0·89	47·88	10·91		19·82	0·12			19·98
	Glass	0·21	50·20	0·65	17·21	7·68		10·50	11·60	2·18		
	Residual	0·0008										
T-2123	Olivine	0·51	40·51			11·51		47·76	0·21			
	Orthopyroxene	0·11	53·56	0·19	5·45	6·93		30·12	2·92			0·82
	Clinopyroxene	0·06	51·19	0·31	7·17	4·58	0·12	18·71	16·85	0·32		1·20
	Spinel	tr.	0·16	0·21	48·24	10·45		19·39	0·06			21·41
	Glass*	0·31	50·18	0·78	17·13	7·83	0·11	9·78	11·84	2·17		0·19
	Residual	0·0093										
T-1493	Olivine	0·42	40·18			11·86		47·19	0·40			
	Orthopyroxene	0·13	52·91	0·21	5·44	7·42		29·91	2·93	0·09		0·95
	Clinopyroxene	0·05	51·54	0·34	6·47	4·62	0·14	18·90	17·38	0·38		0·24
	Spinel	tr.										
	Glass*	0·41	50·20	0·76	17·30	7·63		10·01	11·80	2·16		0·09
	Residual	0·2371										
T-1478	Olivine	0·55	40·40			10·81		48·20	0·29			0·30
	Orthopyroxene	0·12	54·38		3·80	6·84		31·05	2·79			1·14
	Clinopyroxene	0·01	52·26	0·24	5·86	5·44		21·67	13·28	0·24		1·00
	Spinel	tr.										
	Glass*	0·31	50·52	0·68	16·08	7·80	0·12	10·68	12·01	1·90		0·21
	Residual	0·0783										
T-2140	Olivine	0·51	40·79			10·68		48·02	0·28			0·23
	Orthopyroxene	0·04	54·24		4·89	6·49		30·38	2·64			1·36
	Clinopyroxene	0·01	51·44	0·27	6·32	4·82	0·07	19·61	15·43	0·36		1·57
	Spinel	tr.		0·22	36·12	11·10		18·58				33·99
	Glass*	0·43	50·50	0·70	15·80	7·89		10·50	12·32	1·89		0·28
	Residual	0·0335										
T-1464	Olivine	0·54	40·44			10·19		48·97	0·20			0·20
	Orthopyroxene	0·08	55·50		2·98	6·35		32·13	2·17			0·86
	Glass*	0·38	49·84	0·64	15·05	8·34	0·11	12·65	11·48	1·65		0·24
	Residual	0·2409										
T-1480	Olivine	0·56	40·52			10·32		48·68	0·21			0·27
	Orthopyroxene	0·06	55·03		2·98	6·67		31·82	2·35			1·15
	Glass*	0·37	50·20	0·64	14·61	8·49	0·09	12·87	11·13	1·64		0·31
	Residual	0·0746										

APPENDIX B

continued

Run no.	Phase	MB	SiO_2	TiO_2	Al_2O_3	FeO	MnO	MgO	CaO	Na_2O	K_2O	Cr_2O_3
T-1461	Olivine	0·55	40·59			10·39		48·57	0·21			0·24
	Orthopyroxene	0·03	54·64		4·14	6·49		31·18	2·51			1·03
	Glass*	0·41	50·55	0·64	14·22	8·25	0·11	12·88	11·26	1·69		0·40
	Residual	0·0699										
T-2113	Olivine	0·328	40·73			9·82		48·84	0·40			0·22
	Orthopyroxene	0·212	54·89		4·02	5·58		31·41	2·73			1·36
	Clinopyroxene	0·043	51·96	0·19	5·83	4·57		20·84	15·03			1·59
	Spinel	tr.	0·71	0·11	29·72	11·27		16·73	0·27			40·57
	Glass*	0·41	50·17	0·42	15·43	7·68		11·46	13·05	1·21		0·26
	Residual	0·0087										
T-2117	Olivine	0·27	40·22			12·84		46·67	0·27			
	Orthopyroxene	0·21	54·53	0·59	4·12	7·22		29·87	2·53			1·15
	Clinopyroxene	0·10	51·13	1·40	5·92	5·64		19·46	14·57	0·37		1·51
	Glass*	0·41	50·42	3·38	15·56	8·15	0·13	8·22	9·70	3·48	0·76	0·15
	Residual	0·0249										
T-2133	Olivine	0·51	40·84			10·08		48·65	0·21			0·22
	Orthopyroxene	0·09	54·06	0·22	7·26	6·33		29·19	2·51			0·43
	Clinopyroxene	0·11	51·29	0·30	7·00	4·05		19·18	16·81	0·24		1·14
	Spinel	tr.			48·39	9·46		20·58				21·57
	Glass*	0·28	50·01	0·68	17·36	7·13		10·24	12·22	2·05		0·13
	Residual	0·0458										
T-2121	Olivine	0·26	40·69			12·40		46·42	0·36			
	Orthopyroxene	0·21	53·27	0·26	6·79	7·45		28·85	2·74	0·13		0·41
	Clinopyroxene	0·22	50·99	0·34	7·33	4·28	0·04	18·47	16·97	0·37		1·08
	Spinel	tr.		0·31	55·86	10·72		21·53	0·38			11·17
	Plagioclase	0·09	52·21		30·61			0·19	13·60	3·39		
	Glass*	0·20	50·06	1·08	18·00	8·00		9·00	11·20	2·70		
	Residual	0·0154										
T-2078	Olivine	0·28	40·63			10·44		48·66	0·27			
	Orthopyroxene	0·24	54·01	0·23	5·88	6·16		30·14	2·93			0·66
	Clinopyroxene	0·15	50·62	0·36	7·38	4·09	0·07	18·37	17·50	0·50		1·10
	Spinel	0·01	0·27	0·16	53·73	9·80		20·50	0·16			15·30
	Glass*	0·30	49·70	0·88	19·14	7·00		9·11	11·40	2·68		
	Residual	0·0105										
T-2138	Olivine	0·33	41·18			10·03		48·53	0·27			
	Orthopyroxene	0·08	53·74	0·11	5·56	6·38		30·45	2·02	0·05		0·65
	Clinopyroxene	0·09	51·11	0·27	6·37	4·37	0·06	19·48	16·71	0·34		1·30
	Spinel	tr.	0·31	0·23	39·99	10·52		18·78	0·22			29·84
	Glass	0·49	50·73	0·71	17·68	6·67		10·19	11·71	2·19		
	Residual	0·0954										
T-2136	Olivine	0·44	40·96			9·22		49·59	0·24			
	Orthopyroxene	0·07	54·25		4·31	5·33		32·43	2·17			1·51
	Clinopyroxene	0·04	50·20	0·51	7·82	3·85	0·18	18·34	17·46	0·46		1·19
	Spinel	tr.	0·23	0·18	38·76	9·85		18·98	0·21			31·63
	Glass	0·45	50·69	0·70	16·81	6·53		11·14	12·04	1·97		
	Residual	0·0117										

Run no.	Phase	MB	SiO_2	TiO_2	Al_2O_3	FeO	MnO	MgO	CaO	Na_2O	K_2O	Cr_2O_3
Falloon & Green (1988)												
T-1516	Olivine	0·61	40·23			10·78		48·51	0·24			0·24
	Orthopyroxene	0·11	54·23		4·01	6·76		30·91	2·96			1·13
	Clinopyroxene	tr.	51·42	0·29	5·66	4·33		19·36	17·05	0·24		1·64
	Glass*	0·28	51·00	0·78	16·30	7·49		9·90	12·20	2·00		0·38
	Residual	0·1333										
T-1512	Olivine	0·65	40·68			10·11		48·70	0·19			0·32
	Orthopyroxene	tr.	55·00		3·42	6·66		31·40	2·30			1·22
	Glass*	0·36	52·36	0·69	14·43	7·94	0·10	11·12	11·20	1·68		0·48
	Residual	0·1900										
T-1479	Olivine	0·56	40·79			10·12		48·88	0·22			
	Orthopyroxene	0·07	53·91		4·07	6·45		31·89	2·66			1·02
	Glass*	0·36	49·71	0·64	14·38	8·69	0·10	13·22	11·30	1·69		0·28
	Residual	0·2269										
T-1994	Olivine	0·36	41·24			9·43		48·82	0·32			0·19
	Orthopyroxene	0·13	53·87		5·74	5·42		30·81	2·46			1·69
	Clinopyroxene	0·13	52·81	0·19	6·16	4·92		23·70	10·69			1·54
	Glass*	0·38	49·72	0·74	17·50	6·77		10·91	12·02	2·01		0·37
	Residual	0·0066										
T-2189	Olivine	0·30	41·25			9·06		49·25	0·37			
	Orthopyroxene	0·15	54·86	0·14	4·27	5·49		31·28	2·48	0·11		1·36
	Spinel	tr.	0·33	0·20	33·51	10·13		18·41	0·15			37·14
	Glass*	0·54	49·94	0·69	15·08	7·20		12·75	12·25	1·80		0·32
	Residual	0·0252										
T-1989	Olivine	0·227	40·72			11·84		46·68	0·32			
	Orthopyroxene	0·394	52·00	0·28	8·47	7·40		28·44	2·55	0·18		0·58
	Clinopyroxene	0·303	50·96	0·44	8·47	4·96	0·06	18·09	16·35	0·53		0·13
	Spinel	0·025	0·67	0·20	62·35	9·06		21·70	0·15			5·78
	Glass*	0·045	49·80	0·90	18·80	7·30	0·09	9·10	9·30	4·57		0·10
	Residual	0·2776										
T-1999	Olivine	0·32	41·10			9·18		48·75	0·27			0·24
	Orthopyroxene	0·16	53·16	0·20	6·65	5·39		30·15	2·68			1·77
	Clinopyroxene	0·11	52·65	0·17	6·94	5·22		23·39	10·05	0·44		1·14
	Spinel	tr.	0·36	0·15	46·70	8·96		20·08	0·19			23·51
	Glass*	0·41	48·90	0·67	16·00	7·40	0·10	12·69	11·90	1·98		0·33
	Residual	0·0021										
T-2192	Olivine	0·25	41·36			8·53		49·94	0·17			
	Orthopyroxene	0·14	54·89		5·07	5·05		31·32	2·44			1·23
	Glass	0·6	49·19	0·59	14·58	7·36		14·42	11·79	1·67		0·38
	Residual	0·0628										
T-2056	Olivine	0·29	41·41			7·54		50·73	0·32			
	Orthopyroxene	0·21	55·05		4·26	4·77		31·79	2·72			
	Glass	0·49	48·97	0·42	13·77	6·87		15·52	12·98	1·07		
	Residual	3·8554										
T-2029	Olivine	0·25	40·93			11·35		47·49	0·14			
	Orthopyroxene	0·27	53·25		8·17	5·95		29·36	2·48			0·79
	Clinopyroxene	0·35	51·08	0·27	8·21	5·30		21·20	12·53	0·81		0·58
	Spinel	tr.	0·38	0·28	60·49	9·49		21·65	0·11			7·51
	Glass*	0·11	47·4	1·52	17·60	8·7	0·09	10·9	9·5	4·00	0·20	0·10
	Residual	0·0365										

APPENDIX B

continued

Run no.	Phase	MB	SiO_2	TiO_2	Al_2O_3	FeO	MnO	MgO	CaO	Na_2O	K_2O	Cr_2O_3
T-2031	Olivine	0·27	41·01			9·24		48·83	0·23			0·26
	Orthopyroxene	0·24	53·76		6·64	5·40		30·33	2·61			1·27
	Clinopyroxene	0·11	51·43	0·17	7·66	4·56	0·11	21·93	12·31	0·52		1·31
	Spinel	tr.		0·22	52·37	8·14		21·37				17·41
	Glass*	0·37	47·42	0·76	15·3	8·30	0·08	14·19	11·80	1·68	0·03	0·35
	Residual	0·0312										
T-2069	Olivine	0·23	41·29			8·16		50·07	0·20			
	Orthopyroxene	0·23	54·78		4·13	5·28		32·18	2·63			
	Glass	0·52	47·52	0·52	12·96	8·29		17·17	12·09	1·03		
	Residual	1·2042										
T-1515	Olivine	0·54	40·12			11·60		48·10	0·18			
	Orthopyroxene	0·16	52·97	0·09	6·22	6·46		30·20	2·50	0·21		1·20
	Clinopyroxene	0·1	51·97		6·94	5·13		21·18	13·22	0·63		0·94
	Spinel	tr.	0·27	0·20	58·11	9·84		21·43	0·06			10·00
	Glass	0·19	47·03	1·00	16·62	9·67		12·99	9·93	2·63		0·18
	Residual	0·0247										
T-1501	Olivine	0·49	39·70			11·37		48·10	0·35			
	Orthopyroxene	0·19	53·77	0·09	5·90	6·07		30·65	2·40	0·23		0·80
	Clinopyroxene	0·08	50·93	0·14	8·34	5·66	0·06	21·25	12·09	0·69		0·85
	Glass*	0·24	46·30	0·84	15·56	9·88		13·75	11·03	2·08		0·15
	Residual	0·0366										
T-1513	Olivine	0·51	40·39			10·76		48·39	0·27			
	Orthopyroxene	0·14	53·97		5·63	5·96		31·01	2·40			1·03
	Clinopyroxene	0·04	51·57	0·24	7·08	5·58	0·10	22·13	11·90	0·61		0·80
	Glass*	0·31	47·47	0·77	14·51	9·87	0·12	13·89	10·98	2·01		0·37
	Residual	0·0235										
T-1499	Olivine	0·52	40·80			10·19		48·60	0·20			
	Orthopyroxene	0·12	53·43	0·09	6·04	6·27		30·31	2·61	0·17		0·99
	Clinopyroxene	0·08	53·03	0·13	5·74	5·40	0·16	23·60	10·50	0·53		0·90
	Glass*	0·28	46·3	0·81	16·15	10·20	0·13	12·95	10·99	2·25	0·05	0·12
	Residual	0·0374										
T-2207	Olivine	0·47	41·02			9·25		49·30	0·20			0·23
	Orthopyroxene	0·03	54·83		5·00	5·89		31·03	2·07			1·17
	Glass*	0·50	48·60	0·57	12·19	9·60	0·15	17·20	9·60	1·47	0·09	0·43
	Residual	0·1268										
T-2086	Olivine	0·18	41·48			7·71		50·61	0·20			
	Orthopyroxene	0·23	54·00		6·03	4·82		31·71	2·49			0·95
	Clinopyroxene	0·04	52·85		7·30	4·13		24·04	9·90	0·51		1·28
	Glass	0·53	46·86	0·66	13·73	8·06		17·75	10·92	1·60		0·38
	Residual	0·2248										
T-2065	Olivine	0·17	41·51			7·49		50·60	0·19			0·21
	Orthopyroxene	0·24	54·86		5·77	4·31		31·71	2·37			0·97
	Clinopyroxene	tr.	53·25		6·85	4·07		25·34	8·73	0·53		1·24
	Glass	0·59	46·72	0·55	12·72	8·40		19·31	10·59	1·18		0·51
	Residual	0·0768										
T-2075	Olivine	0·11	41·35			7·08		51·13	0·20			0·23
	Orthopyroxene	0·18	55·65		4·65	4·23		32·60	2·15			0·72
	Glass	0·7	46·99	0·50	12·21	8·09		20·23	10·12	1·31		0·52
	Residual	0·0622										
T-2087	Olivine	0·19	41·35			7·97		50·47	0·21			
	Orthopyroxene	0·23	55·82		4·76	4·60		32·02	2·14			0·64
	Clinopyroxene	0·07	53·82	0·23	6·47	4·21		24·22	9·47	0·99		0·59
	Garnet	0·05	42·23	0·47	22·95	5·88		22·06	5·12			1·29
	Glass	0·46	45·83	1·08	11·70	9·04		19·99	10·66	1·36		0·33
	Residual	0·1368										

Mass balance (MB) in weight fraction was performed using least-squares linear regression using the software Petmix and 'Residual' refers to the square of the sum of the residuals.
*Reanalysed glass composition (this study).